TAMPEREEN TEKNILLINEN YLIOPISTO
TAMPERE UNIVERSITY OF TECHNOLOGY

MITHILESH PRAKASH

GEOMETRICAL MEASUREMENTS OF ORTHOGNATHIC SURGERY CHANGE USING CONE BEAM COMPUTED TOMOGRAPHY

Master of Science thesis

Examiner: prof. Hannu Eskola
Examiner and topic approved by the Faculty Council of the Faculty of Natural Sciences
on 14th January 2015

ABSTRACT

Mithilesh Prakash: Geometrical Measurements of Orthognathic Surgery Change Using Cone Beam Computed Tomography
Tampere University of technology
Master of Science Thesis, 54 pages, 18 Appendix pages
March 2015
Master's Degree Programme in Biomedical Engineering
Major: Medical Physics
Examiner: Professor Hannu Eskola

Keywords: CBCT, Superimposition of CBCT, Orthognathic surgery

Imaging in the three dimensional format, Cone Beam Computed Tomography has become quite popular in orthodontics. Tools for analyzing the volumetric data however have not caught up with the recent industry demands. Most of the analysis in 3D is primarily based on techniques used in 2D format, thus adding some limitations to the post diagnostic capabilities of the imaging modality. Currently there is no dedicated tool or a stand-alone automated technique to capture the geometry of the CBCT volumes. The purpose of this study is to explore a method to measure the geometry of the CBCT volumes and find the changes in the orthodontics after the surgery, all in a technically non-intensive and reproducible way, thereby paving way for further developments of dedicated analysis tools in this field.

Anonymized sequential CBCT volumes of subjects prior to and after the surgery were obtained from the University of Tampere Hospital's radiology department. The volume sets of the subjects were loaded into AMIRA software tool, resampling if the volumes were not of similar dimensions, superimposed with mutual information algorithm, segmenting required volumes for 3D rendering, attaching landmarks to specific locations and measuring the geometries from the landmarks. The method was then put into a step by step guide with minimum technical knowhow for usage by the medical personnel.

PREFACE

Firstly, I would like to thank Professor Hannu Eskola for providing me an opportunity to take up this thesis and for trusting in my capabilities to complete the same. Your keen interest in the medical physics is truly inspiring and helped me to remain motivated throughout.

I would to like thanks Professor Timo Peltomäki and Dr. Jukka Kurimo for helping me in understanding the topic and clarifying in various discussions over the product development period. Your inputs on approaching the thesis and suggested papers were invaluable. Thanks for your continued support.

Special thanks to Dr. Jorma Järnstedt for providing me access to datasets and introducing me to the facility at the Tampere University hospital.

Also, the thesis work was financially supported by the Competitive State research financing of the Expert Responsibility area of Tampere University Hospital, Grant 9R004.

Tampere, 18.3.2015

Mithilesh Prakash

CONTENTS

1. INTRODUCTION 8
2. LITERATURE REVIEW 10
2.1 X-ray Imaging, Computed Tomography and CBCT 10
2.2 Limitations of CBCT 13
2.3 Reliability of measurement by CBCT 15
2.4 3D Image processing techniques 17
2.4.1 3D Image filtering using Gaussian distribution 17
2.4.2 Surface and Volume rendering 17
2.4.3 Image segmentation 17
2.4.4 Registration of images 18
2.5 Orthognathic Surgery 19
2.6 Measurements of Orthognathic Surgery 21
3. AIM OF THE WORK 23
4. MATERIAL AND METHODS 24
4.1 Subjects 24
4.2 Imaging procedure 24
4.3 Filtering, cropping and centre alignment of the data sets 26
4.4 Superposition of cropped datasets 27
4.5 3D Volume rendering 28
4.5.1 Segmentation of the registered datasets 28
4.5.2 Segmentation accuracy 28
4.6 Landmarks and measurement procedure 29
5. RESULTS 33
5.1 Segmentation analysis 33
5.2 Superimposition analysis 36
5.3 Geometrical calculations analysis 38
5.4 Surgery change estimation analysis 40
5.5 Calibration and Validation of measurements 42
6. DISCUSSION 45
6.1 Anonymized data 45
6.2 Processing of collected data 46
6.3 Segmentation of 3D volumes 46
6.4 Geometrical calculations 48
6.5 Accuracy and limitations 50
6.6 Methodology summary 52
6.7 Scope for future improvements 53
7. CONCLUSION 54

APPENDIX A: Amira application guide limited to thesis methodology.

LIST OF FIGURES

Figure 1: X-ray tube [3] *10*
Figure 2: X-ray functional block diagram [4] *10*
Figure 3: Evolution of four generations of CT scanners [6] *11*
Figure 4: X-ray CT vs. CBCT imaging modality [10] *12*
Figure 5: Cone-beam effect origins [1]. *14*
Figure 6: Comparison of CBCT image data with actual images. Cross-sectional images on the right side in the second molar region. A, cone beam CT (CBCT) image of dry mandible; B, CBCT image of mandible in sucrose solution; C, multislice CT (MSCT) images of dry mandible; D, MSCT images of mandible in sucrose solution using conventional scanning parameters SE 759; E, low-dose MSCT images of mandible in sucrose solution SE 905 [16] *15*
Figure 7: Types of Orthognathic Surgery [25] *19*
Figure 8: Typical steps in computer assisted surgery in orthodontics [24] *20*
Figure 9: Flowchart of method for superimposition of CBCT scans as presented by Cevindanes et al 2005 ..... *21*
Figure 10: Imaging equipment used for imaging acquisitions, Planmeca ProMax 3D Max [30] *25*
Figure 11: Alignment of cropped datasets for superposition process. Each scan is color coded differently. Green model is of presurgery and white model is of postsurgery scan. *26*
Figure 12: Superimposed datasets after affine registration. Both the scans in the dataset are of gray scale. As shown above the upper regions coincide representing no changes, while the lower region a little blurred showing mismatch in the scans due to effects of the surgery. *27*
Figure 13: Anatomy of the lower Jaw. *29*
Figure 14: Landmarks placement on the various sections of the segmented 3D volume. Landmarks are shown in golden points. *30*
Figure 15: Landmarks points with mapping structure to capture both upper jaw and lower jaw measurements *31*
Figure 16: Mapping structure without the segmented 3D volume data. *31*
Figure 17: The above figure shown segmentation view for presurgery scans (a, b, c), postsurgery (d, e, f) and superimposed scans (g, h, i). Some sections of the scans are missing showing the limitations of the segmentation process. *34*
Figure 18: Surface distance 3D models illustrating the inter-user differences in segmentation. The map primarily consists of blue vector arrows indicating minimum surface distance or differences between the segmented models. *35*

Figure 19: Surface distance measure analysis. The models are made of vectors pointing the direction of change in the surface distance with respect to presurgery model. The scale is as given in (e) and the zoomed in version is seen in figure (f). *37*
Figure 20: Example of mapping of the skull with landmarks and various inter-landmark distances. *38*
Figure 21: The mapping skeleton of the skull without the 3D model. *39*
Figure 22: Sample data with mapping on Presurgery and Postsurgery 3D model. *40*
Figure 23: Phantom model used for testing the measurements *42*
Figure 24: Noisy projections at the intersections of the upper and lower jaw. *47*
Figure 25: The surgery change markers and splint imprints visible in the segmented models of the postsurgery scans. *47*
Figure 26: Landmarks from the dataset scans, some points in the upper section are closer than the lower section where there is definte change in the position. This also depicts the ability to superimpose the landmarks before the actual measurement is done. *49*
Figure 27: Inter-Landmarks mapping from Presurgery and Postsurgery models. *50*
Figure 28: Essential steps in the method used to find the geometry of the CBCT scans. *52*

LIST OF TABLES

Table 1: Statistical information indicating inter-user differences for segmentation.....35
Table 2: Superimposition statistical information for the dataset shown in figure 19.....36
Table 3: Assessment of the surgical changes utilizing the data from the models as shown in the previous figure is illustrated. The table shows the difference in lengths in various sections of the skull. For simplicity only distance measurements are considered.....41
Table 4: Statistical analysis of the measurements between ImageJ and AMIRA 43
Table 5: Surface distances for different subjects showing sub-voxel accuracies.....50

LIST OF SYMBOLS AND ABBREVIATIONS

2D	Two dimensional
3D	Three dimensional
CBCT	Cone beam computed tomography
CMM	Coordinate measuring machine
CT	Computed tomography
Dataset	Set of two CBCT scans taken before and after the surgery
FOV	Field of view
HU	Hounsfield unit
MM	Millimeter
MRI	Magnetic resonance image
OMF	Oral and maxillofacial
Orthognathic Surgery	Surgery in the OMF region
Postsurgery	After the surgery
Presurgery	Before the surgery
ROI	Region of interest

1. INTRODUCTION

Imaging is an important diagnostic tool in the medical field. Recent advances in the 3D technologies have resulted in wonderful visual representations of the human anatomy. Most of the attempts to understand the human anatomy are still primarily done in 2D due to its gross simplicity and availability of well-established methods. As non-invasive imaging technology progresses acquisitions are reaching near perfection but the evolution of tools to analyze in 3D is lagging.

Cone beam computed tomography (CBCT) is a recent technology but has gained widespread popularity in the dentistry. CBCT marks the shift from 2D to 3D approach in the imaging technology right from image acquisition to its reconstruction. Imaging is achieved by a rotating gantry model which has both x-ray source and detector. A cone shaped divergent radiation beam is projected through the area of interest and on to the detector [1]. Imaging is completed usually in one full rotation.

CBCT produces excellent image quality and surface rendering from captured volumes, but due to increased radiation exposure comparatively to other modalities, CBCT is prescribed only when necessary. As newer 3D imaging technologies evolve so must the technology of analytics for a comprehensive diagnostic ecosystem development. Currently, 3D analysis is largely dependent on existing 2D analytical methods thus provide no significant advantage for moving in 3D. To gain deeper understandings and unlock newer potential in the 3D technology, newer methods to analyze in 3D must be developed.

A study to establish an easily reproducible and technically non-intensive method of performing geometrical measurements of volume data resulting from CBCT scans is discussed. Through the measurements of the CBCT scans in 3D, assessments of orthognathic changes after the surgery can be estimated with fair accuracy.

The dental surgeons at the Tampere University Hospital faced the problem of finding the right tool to perform measurement changes in 3D of the CBCT scans of patients undergoing orthognathic surgery. This project explores a method to solve the problem stated and lay the footprints of future development of such standalone tools.

The report begins with providing the literature review providing background information introducing the concept of X-ray imaging, CBCT and orthognathic surgery. Next the aim of the thesis is stated followed up with materials and methods used to carry out the product development. The materials and method section presents the steps

and the concepts used to fulfill the aim of the thesis. Next the results of the thesis are discussed with illustration and tabulated information of sample datasets. Then the results are discussed in quite detail presenting information and experiences obtained during the course of product development. The discussion section also contains information on how the method developed was validated and tested.

The thesis report concludes by discussing the objectives achieved and scope for further improvements. A guided step-by-step manual is included in the appendix section fine-tuned to perform the activities of the thesis.

2. LITERATURE REVIEW

2.1 X-ray Imaging, Computed Tomography and CBCT

The discovery of X-rays in the late 18th century changed the medical diagnostics significantly. The ability to see structures within the skin non-invasively saved time and money, this marked one of the stepping stones into the medical imaging domain. Orthodontics found significant usage of x-ray imaging.

A conventional X-ray tube device consists of a metallic filament (emitter) called the cathode, which is heated over 1000 ^{O}C and a metallic receptor called the anode, which when bombarded with by accelerated electrons from the emitter, produces X-rays. The design has not changed significantly in over a century [2]. The diagram of a simple X-ray tube and modern medical imaging device is as shown in figures 1 and 2.

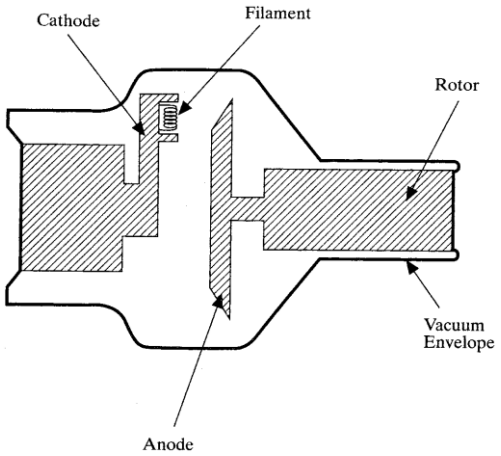

Figure 1: X-ray tube [3]

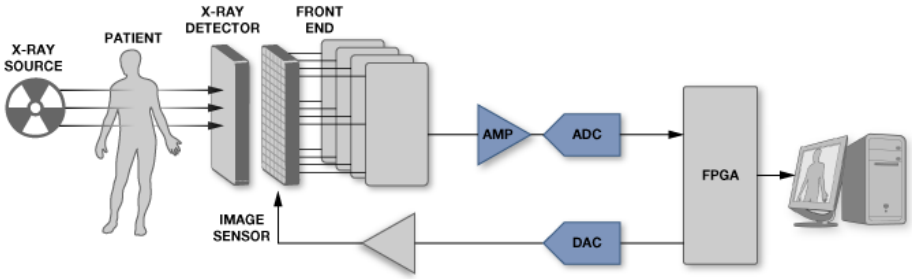

Figure 2: X-ray functional block diagram [4]

X-ray computed tomography (CT) was the first slice-imaging type medical device, marking the modern era of imaging modality, was introduced in the late 1900's. CT only became feasible after advent of computer technology in the 1960's. CT ever since its introduction has shown significant technological progress, clinical demands and also survived the time when magnetic resonance imaging was gaining popularity. The real push in CT's application came though when spiral scanning was invented. This invention marked the shift from slice to volume imaging. Henceforth whole body imaging applications was a possibility in less than 20 seconds with improved isotropic resolution, complemented with array detection technology [5]. The CT development over the years can be summarized in the figure 3 below.

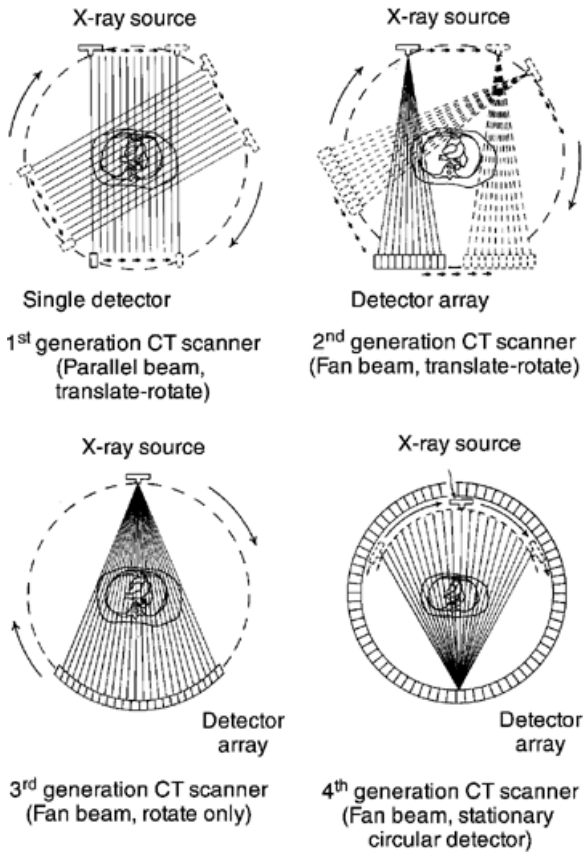

Figure 3: Evolution of four generations of CT scanners [6]

Cone-beam computed tomography (CBCT) is the next step from mainstream CT technology. CBCT is a medical imaging modality based on acquisition using cone shaped X-ray beam centered on the detector array arranged two dimensionally. The three dimensional volume data is calculated from the acquired 2D data using the Feldkamp et al algorithm. Due to the size and radiation dose CBCT gained popularity in oral and maxillofacial (OMF) surgery [7] , orthodontics and dentistry [8]. It was in late 1990's the working model of CBCT was independently developed in Japan and Italy [9].

CBCT modality saw a rapid rise in the technological aspect from the first prototype to faster and application specific scanners. The figure 4 shows comparison of conventional CT and CBCT scanners.

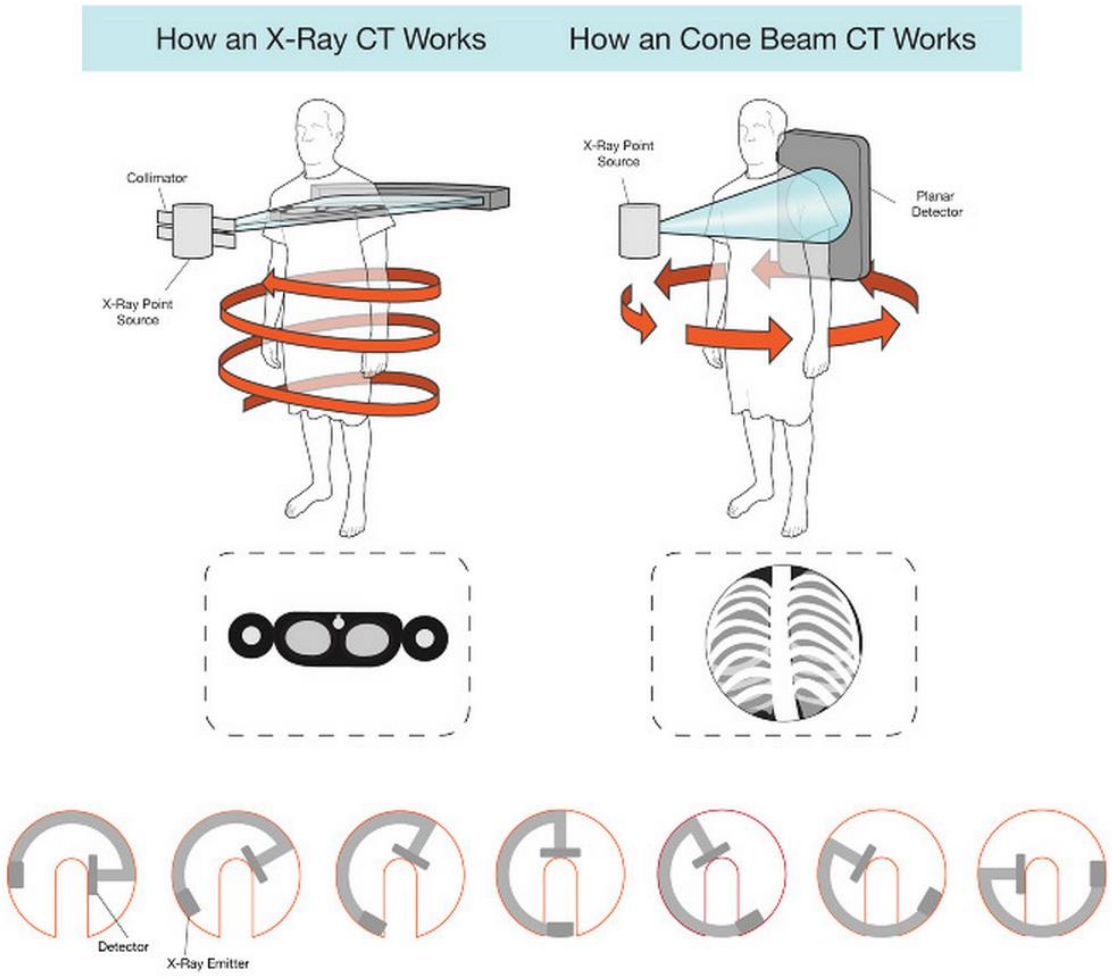

Figure 4: X-ray CT vs. CBCT imaging modality [10]

2.2 Limitations of CBCT

CBCT imaging modality is mainly restricted to quality of the image in comparison with noise and the amount of scatter radiation affecting the contrast resolution. Poor tissue contrast, noise and artifacts affect the clarity of the CBCT output [1].

Artifacts: Any error or distortion in the CBCT output not related to the subject being examined is classified as artifacts [11].

X-ray beam artifacts: Artifacts in CT arise due to beam hardening cause due to inherent polychromatic nature of the X-ray. Beam hardening gives rise to two types of artifacts. The first type is cupping artifact due to differential absorption by metallic implants. The second type is in the form of dark bands and streaks which tend to appear between two dense objects. These effects are more pronounced in CBCT than in CT due to heterochromatic x-ray beam and lower peak energy (kilovolt) than CT. However these artifacts can be digitally processed and are reduced in reconstruction algorithms.

Motion artifacts: Patient movements during scanning can cause misregistration of data. This can be controlled using a head restraint and shortening the scanning time [12].

Scanner-related artifacts: Poor calibration and inherent circular shape of the scanner introduces artifacts. This type effect is called circular effect.

Cone-beam artifacts: The geometry of the cone beam introduces three types artifacts clinically observed. These are partial volume averaging, under sampling and cone-beam effect. These effects can be easily countered by signal processing.

Partial volume averaging: When the selected voxel resolution of the scan is greater than the spatial or contrast resolution of the object to be scanned, partial volume averaging occurs [13]. This is common feature in conventional fan and CBCT imaging. This artifact is predominant in regions where surfaces change rapidly in the z-direction. Selecting the smallest acquisition voxel can reduce this type of artifact.

Under-sampling: Occurs during reconstruction if there are only few projections available to represent the data. Misregistration of images can occur along with the development of sharp edges. This can be avoided by having sufficient number of projections.

Cone-beam effect: The cone beam geometry is a potential artifact source more so in the peripheral region of the scan volume. Due to divergence of the x-ray beam as it rotates around the subject in the horizontal plane, data of the projections are collected by each detector pixel. The feature of the artifacts is more explicitly shown graphically in figure 5. Many counter methods include cone beam adjusted reconstruction algorithms and positioning the region of interest visible in the horizontal plane and FOV selection.

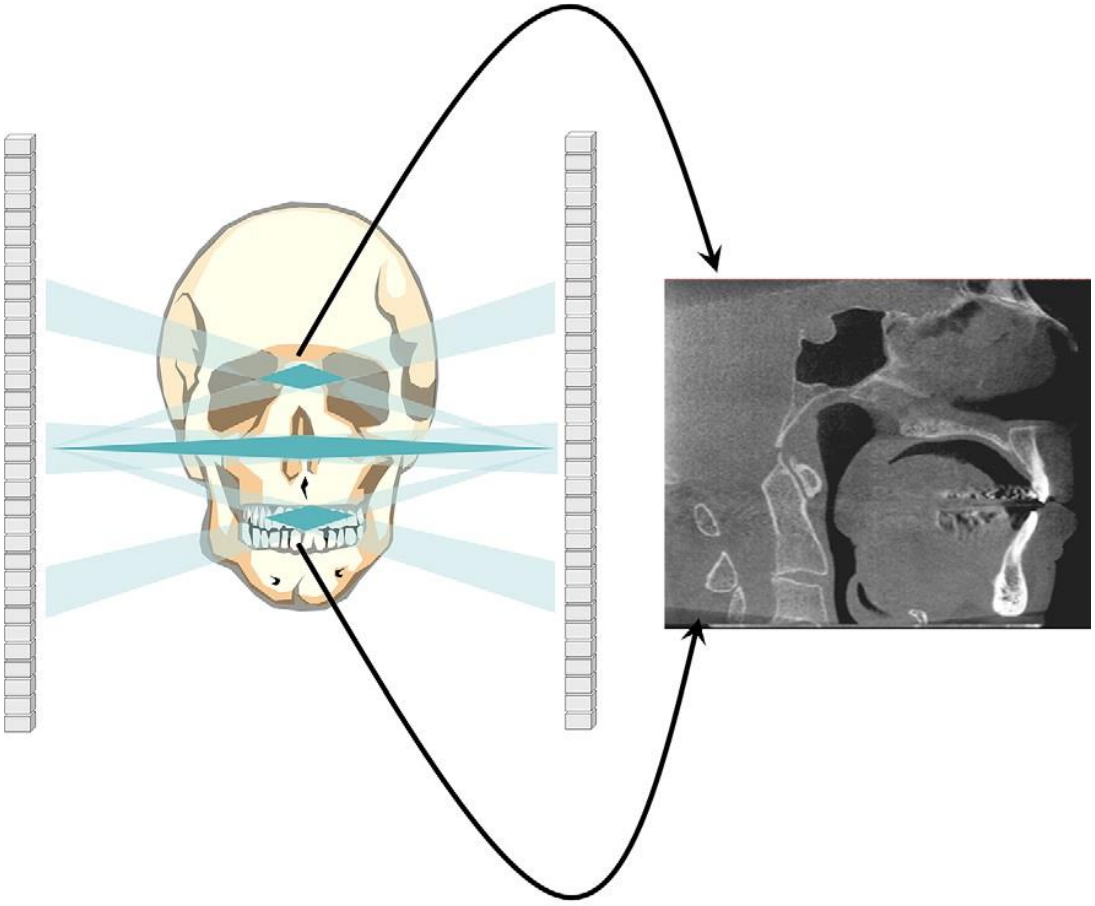

Figure 5: Cone-beam effect origins [1].

The figure above shows, the projections of three x-ray beams, one perpendicular, one angled inferiorly, and the other angled superiorly, from a point origin are shown at two positions of the x-ray tube, exactly 180^{o} apart. The amount of data collected by the detector for reconstruction corresponds to the solid volume between the overlapping projections. Centrally, the amount of data acquired is maximal, whereas peripherally, the amount of data collected is appreciably less. The midsagittal section image demonstrates the visual effects of this in producing a peripheral ‘‘V’’ artifact of increased noise, distortion, and reduced contrast (*Quoted from* [1]).

2.3 Reliability of measurement by CBCT

After considering the limitations and various artifacts in the CBCT, next logical question to ponder upon is the accuracy and reliability of CBCT in providing geometrical measurements. The dimensions of the skull have been quite accurately measured by anthropologist on the dry skulls. With the development of imaging modalities measuring the skulls of living subjects gained popularity ever since discovery of x-rays. 2D x-ray measurements provided good accuracy and have stood the test of times.

Many researches have been done testing the accuracy of the CBCT measurements. In one of the studies as shown by Manuel et al ([14] describes the method to validate the software measurements with coordinate measuring machine (CMM). The results were very close. Similar works were performed by Periago et al [15] and results were accurate. Figure 6 shows one such research using multislice CT as described by Suomalainen et al.

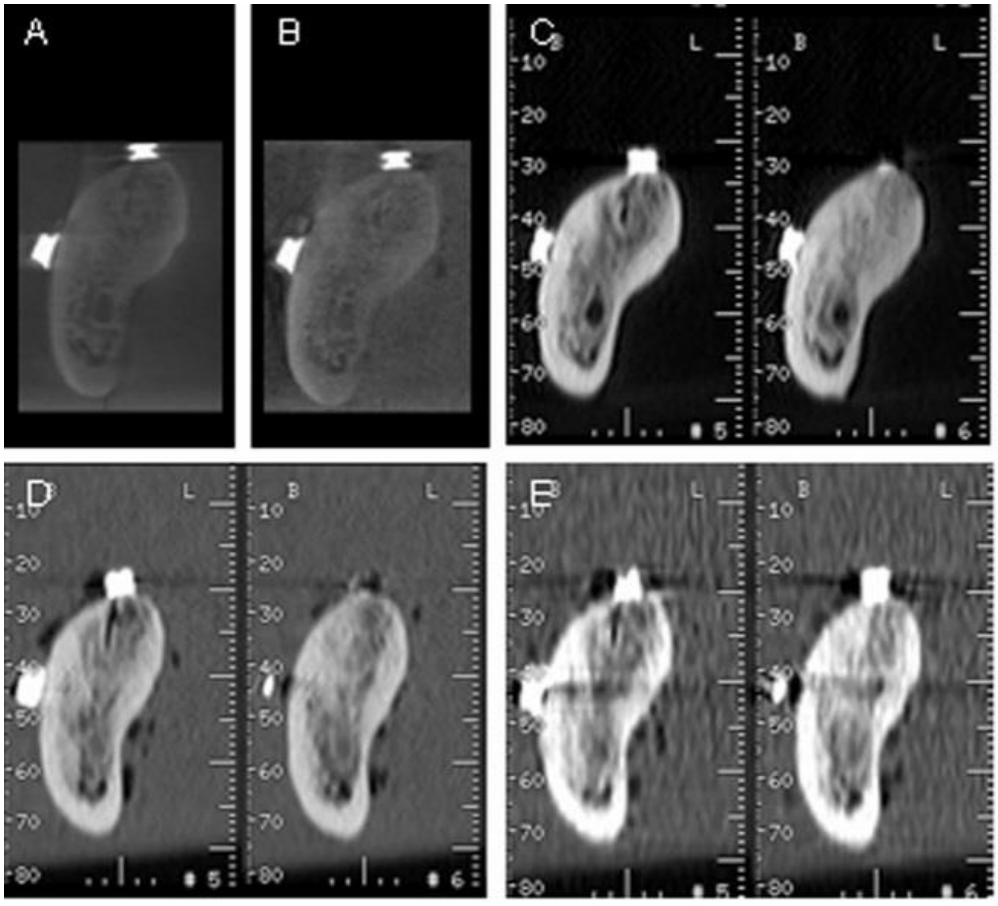

Figure 6: Comparison of CBCT image data with actual images. Figure shows cross-sectional images on the right side in the second molar region. A, cone beam CT (CBCT) image of dry mandible; B, CBCT image of mandible in sucrose solution; C, multislice CT (MSCT) images of dry mandible; D, MSCT images of mandible in sucrose solution using conventional scanning parameters SE 759; E, low-dose MSCT images of mandible in sucrose solution SE 905 [16]

Hence most of the CBCT measurements can be considered clinically accurate [17], but much of the usage of the measurement data is still at the discretion of the practitioner [18].

2.4 3D Image processing techniques

CBCT volume data presents stack of slices of data in 2D. By digital manipulation of the stacked data 3D model can be reconstructed. Open-source software is freely available on the web to visualize CBCT data; the list includes 3DSclicer, Seg3D and the very popular ITK-SNAP. The open-source software comes with free access to source code so customized software can be freely created and distributed. The software discussed in the list was fully funded by National Institutes of Health (NIH, U.S.A).

Open-source software requires software expertise to develop customized applications and tools to handle 3D images such as CBCT. Several commercial software such as Anatomage, CyberMed and Amira offer easy graphical user interface to develop networks to manipulate the 3D data.

This section of the thesis introduces the various concepts of digital image processing techniques used to fulfill the objectives.

2.4.1 3D Image filtering using Gaussian distribution

The digital smoothing algorithm is simple conceptually but very effective in smoothing the noisy CBCT 3D images. The algorithm is based on sigma probability of the Gaussian distribution and it smoothens out every pixel in the sigma range [19]. The image edges, the outline and essential features are retained in the image.

2.4.2 Surface and Volume rendering

The visualization of different structures in the CBCT volumes can be done by selecting the intensity levels of the region of interest. Multiple structures can be selected by appropriately color coding the surfaces. In case of surface rendering entire volumes of similar intensities appear as mono color mono surface structure. The final output essentially depends on the homogeneity of the CBCT data [20]; else the surface will be discontinuous.

Volume rendering highlights entire volumes and but unlike surface rendering transparencies is controlled to differentiate between volumes. The conventional method of grey scale is preferred method.

2.4.3 Image segmentation

Most medical image processing applications usually involves some level of segmentation to analyze the region of interest. Segmentation is a process of delineating the entire picture and focusing on the segments of the medical image to measure the size and

shape of the structures such as tumor growth or spread in a MRI scan. This is done by active contour processing algorithms either initiated manually or automatically [21].

2.4.4 Registration of images

Registration is a process of overlapping two or sometimes more images on top of one another usually taken in similar imaging conditions [22]. This process is crucial since the variations in the images is quite apparent and thus helps in the detection of changes in the imaged scenes [23].

Many algorithms are developed to tackle the registration problem. Rigid registration provides the best approach since the scale of the images registered is not compromised.

2.5 Orthognathic Surgery

Orthognathic surgery involves repositioning of certain sections of the jaws. Depending on the need either of the jaws or both the jaws can undergo surgical operation. Reconstruction type of surgery entails replacing missing or damaged section of OMF region with implants or grafts [24]. The figure 7 shows examples of different types of orthognathic surgery.

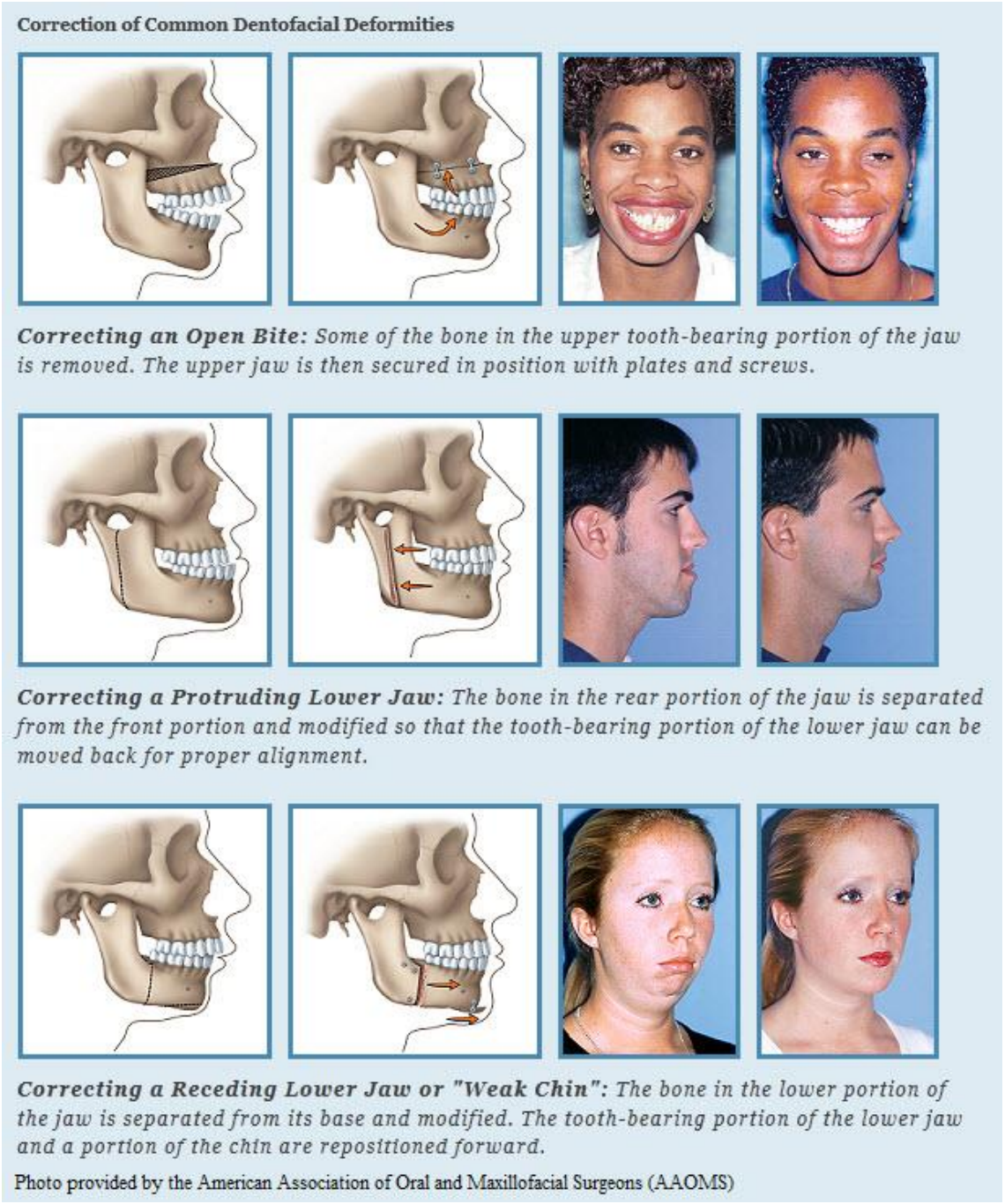

Figure 7: Types of Orthognathic Surgery [25]

Orthognathic surgery is performed for medical and non-medical reasons. Medical reasons include apnea condition correction, dislocation due to accident, chronic mouth breathing and dry mouth, difficulty in chewing and swallowing (mastication) etc. Non-medical reasons include correcting birth deformities, esthetic appearances, receding jaw, protruding chin etc. Dental surgeons generally find large number of surgery for medical reasons.

Medical terminologies commonly used by dental surgeons describe the location and extent of the surgery. If only lower jaw is operated it is termed as bilateral sagittal split osteotomy. Upper jaw surgery is called LeFort 1osteotomy [26]. And finally if both the jaws are operated then the surgery is termed as bi-maxillary osteotomy.

Orthodontics has significantly received boost with advancement in CBCT technology, computational algorithms and communications systems. Each patient in OMF surgery has unique dimension and needs careful planning or the surgery and splint's design and specification. CBCT now helps the designers and surgeons to plan the surgery and design the implants to individual specification. Computer assisted surgery can also be used with the acquired scans thus improving the accuracy of the surgery to certain extent [27]. The figure 8 shows the general process of in a typical surgery in modern day orthodontics.

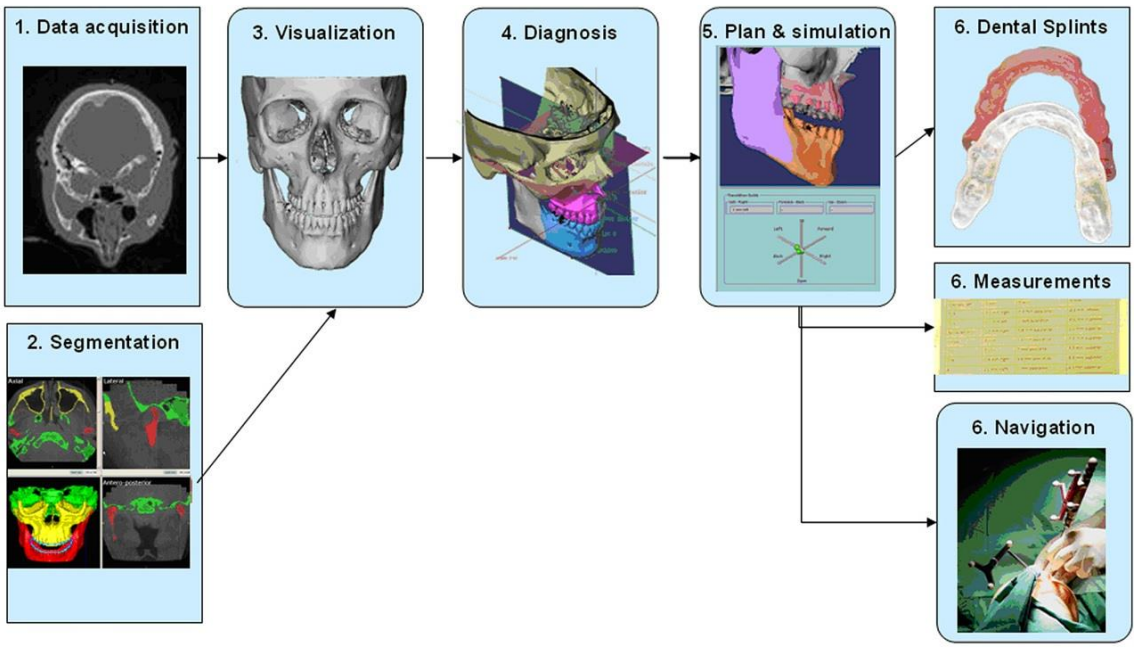

Figure 8: Typical steps in computer assisted surgery in orthodontics [24]

2.6 Measurements of Orthognathic Surgery

Orthognathic CBCT scan measurement is the next logical step in the orthodontics to not only plan and execute the surgery but also to assess the changes the surgery has resulted in. The standard technique of the measuring the CBCT scans to assess the surgery changes are to superimpose the scans taken before and after the surgery and then assess the 3D projections.

Cevidanes et al 2005 in the paper published under the name "Three-dimensional cone-beam computed tomography for assessment of mandibular changes after orthognathic surgery". The steps can be illustrated as shown below in the schematic diagram in the figure 9.

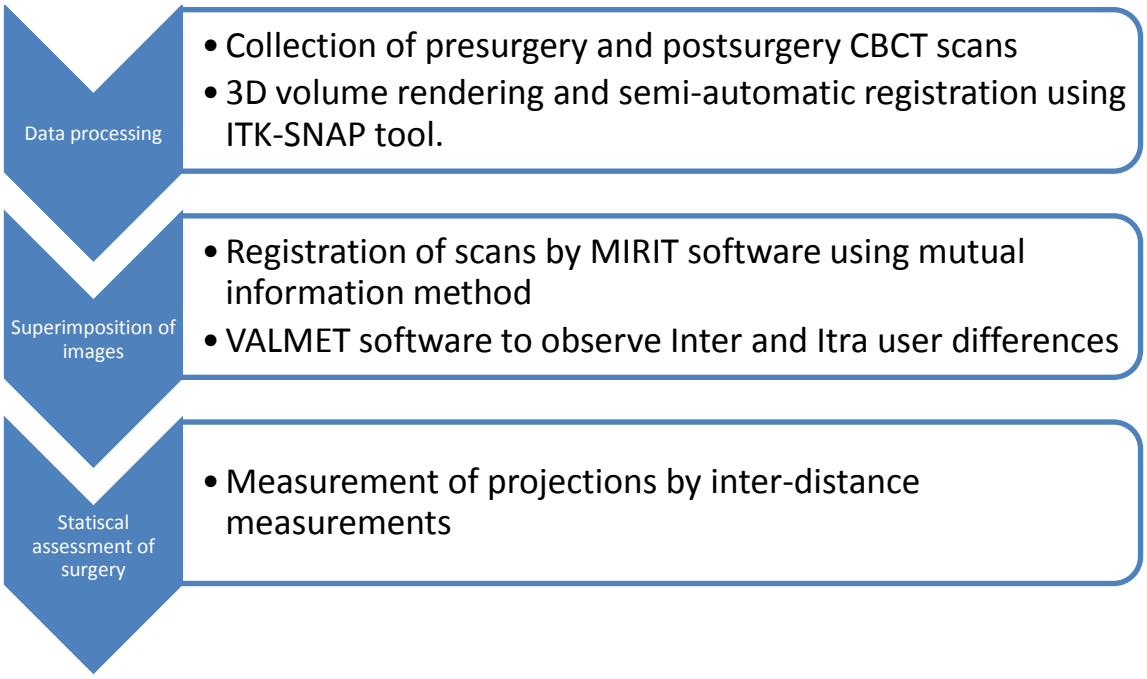

Figure 9: Flowchart of method for superimposition of CBCT scans as presented by Cevindanes et al 2005

The study was comprehensive but many of the software segments like MIRIT and VALMET are no longer available. Also the method does not fit in one single integrated package and requires high level of software designing and programming which is out-side the scope of current clinical routine.

Another research by Maal et al [28] performed an assessment of human dry skulls in the paper "A comparison between 2D and 3D cephalometry on CBCT scans of human skulls". This study evaluated if the measurements from conventional cephalometric ra-diographs were comparable with the 3D measurements using 3D data from CBCT. The method explored inter-observer differences and was found be in the range of 0.69 to 0.91, which was under acceptable limits. The results of the main purpose of comparing 2D imaging and 3D imaging however had significant influences on the reliability of

CBCT in using for measurement purposes. The CBCT or 3D measurements and 2D cephalometric measurements differed only on a small range.

Similar study by Sebastian et al [29] measured the reliability and accuracy by using 3D CBCT images and reconstructing various sections of the 3D skull model and comparing it with digital caliper. The digital caliper was used as a gold standard for measuring inter-tooth measurement and later comparing with 3D image measurements. This was in line with previous researches done so far. The findings were similar to works done by Lascala et al [17].

Thus, the above results and methodology support the usage of CBCT for clinical usage in orthognathic measurements. But more such studies are required to deem the measurements to be used in actual practices since the results are close to actual measurements but some degree of error still do persist.

3. AIM OF THE WORK

The aim of the thesis is to fulfil the following objectives:

1. Develop an easy to use tool to measure in 3D the geometry of the CBCT volumes taken before and after the orthognathic surgery.
2. Assess the changes of the orthognathic surgery.
3. Create an easy to follow guide with step-by-step instructions with minimal technical know-how.

4. MATERIAL AND METHODS

4.1 Subjects

Anonymized CBCT scans of subjects undergoing orthognathic surgery were obtained from the radiology department of Tampere University Hospital. Since the method to be developed was aimed for universal application, no selection criteria were imposed on subject's sex, age or type of orthognathic surgery in the scans selection. A dataset in this method was defined as a pair of CBCT scans taken before and after the surgery of the same subject. However, the only precondition during the product development was that the data sets used for selection were acquired with same CBCT equipment under similar imaging settings and conditions.

Data sets acquired from different CBCT equipment or under different imaging setups were eliminated. Also different positions of the subject in the scan data set were eliminated due to difficulty in registration process.

After the process of elimination eight data sets were finalized for product development. The data sets were of different surgery types thus allowing the method to demonstrate its robustness and universal application.

4.2 Imaging procedure

The data set scans were acquired using "Planmeca ProMax 3D Max" CBCT equipment, specialized for orthognathic scans. The device is capable of capturing both 2D and 3D images. The CBCT model used is tailor made for dentistry with various pre-set programs. The scans were stored as series of 2D image slices in the standard DICOM format.

Figure 10 in the next page shows the CBCT imaging equipment model used in the image acquisitions for product development method used in this thesis work.

Figure 10: Imaging equipment used for imaging acquisitions, Planmeca ProMax 3D Max [30]

The data sets used in this product development study were of 575x575x575 slices with 0.4 millimeter voxel size.

4.3 Filtering, cropping and centre alignment of the data sets

The datasets were imported to the AMIRA software. The data sets were then digitally filtered and smoothed out with Gaussian smoothing process using the built-in filter mechanism. This process smoothens out the rough noisy image projections in 3D. The datasets are then aligned for the centre of the axis to match. The alignment of cropped data is shown in the figure 11.

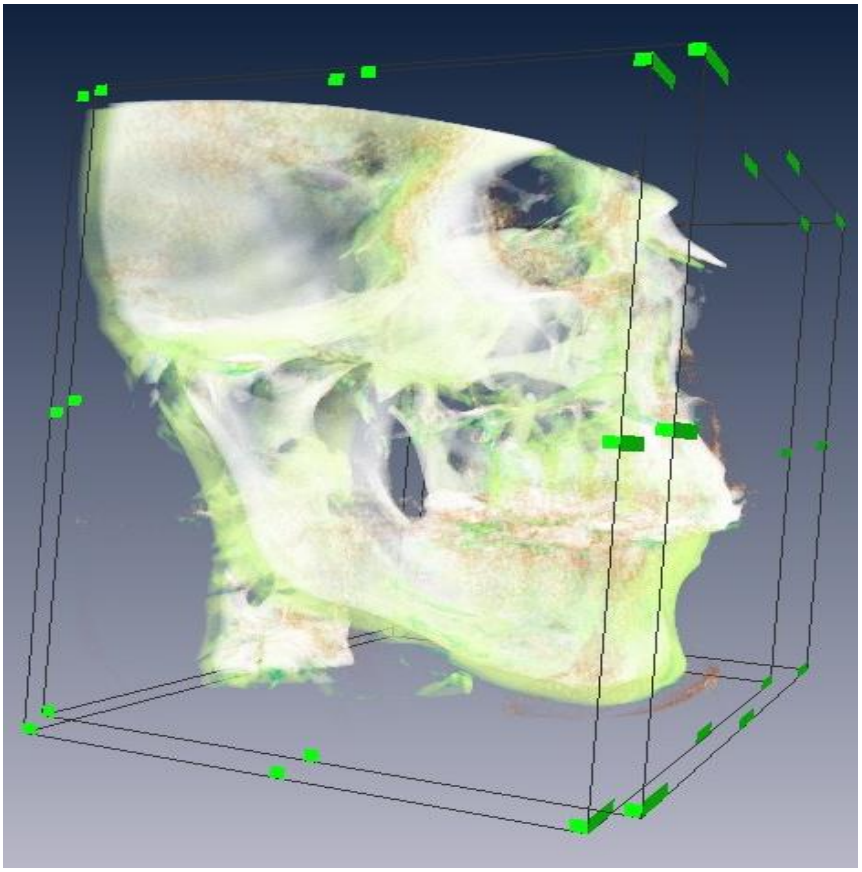

Figure 11: Alignment of cropped datasets for superposition process. Each scan is color coded differently. Green model is of presurgery and white model is of postsurgery scan.

4.4 Superposition of cropped datasets

The cropped datasets are manually aligned roughly by rotation and translation tools in the user interface, if the skull models are found be too off-centre. The datasets are then superimposed using rigid registration process. Once the centres and skull models are visually aligned roughly, the automated tool in the Amira's Affine Registration module is used. This module computes an affine transformation for the co-registration of two image data sets, using an iterative optimization algorithm. Affine registration aligns the datasets in comprehensive fashion taking the sum over squared differences and measuring the mutual information. Once the datasets are registered segmentation process can begin. Figure 12 shows the datasets after affine registration.

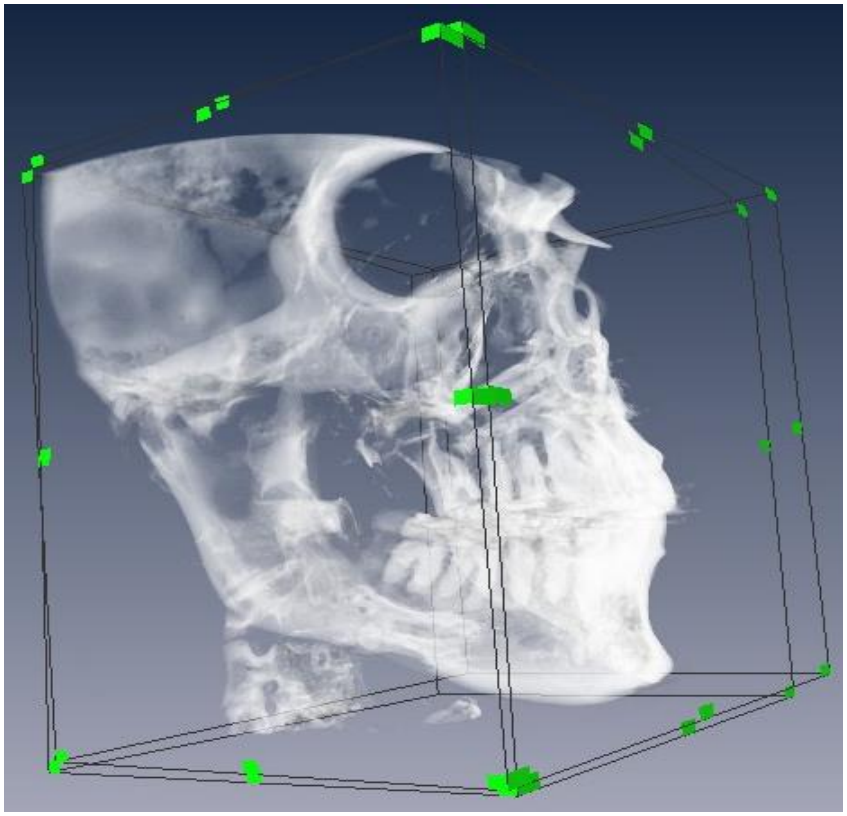

Figure 12: Superimposed datasets after affine registration. Both the scans in the dataset are of gray scale. As shown above the upper regions coincide representing no changes, while the lower region a little blurred showing mismatch in the scans due to effects of the surgery.

4.5 3D Volume rendering

Volume rendering is process of visualising the data 3 dimensionally. For this process commercially available tool (AMIRA, version 5.3.3) was used. The steps involved in 3D volume rendering are discussed in this section.

4.5.1 Segmentation of the registered datasets

The registration of the datasets statistically aligns the models and hence segmentation process can be initiated. Segmentation process helps in selecting the bony structures of the skull and hence filters all background and foreground information.

Segmentation is initiated manually by selecting the intensity levels in the labels editor in the segmentation module. Voxels with grey values corresponding to the jaw section is identified. The threshold of the grey values in the range -3000 to 1000 HU are chosen. The sections of the skull appropriate to bony sections and jaw are selected. Then the software matches the intensities over the entire 3D section. The user interface depicts the model in 3D and sections can be adjusted by narrowing the window size of iterations. This process results in a 3D model of CBCT scans. Both the scans dataset are segmented using this process.

During the process of the segmentation the datasets are colour coded. In this product development and figures that follow, green was selected for presurgery model and red for postsurgery model.

4.5.2 Segmentation accuracy

The process of segmentation requires manual selection of intensity and window size. As result no two segmentation models can be identical if proper care is not taken. But with sufficient practice the segmentation process can be fairly quickly and accurately done. The measurement of the skull changes by a negligible amount due to inter-user changes in the segmentation process.

The segmentation process was locally tested to simulate the inter-user changes. The testing procedure and results are discussed in detail in the results section of this report.

4.6 Landmarks and measurement procedure

The measurement procedure presented few challenges in determining the method to select the dimensions for measurement. Previously no standards or methods for skull measurement to fulfil the objectives were found. The mapping of skull to assess the surgical changes was not established. This section provides a novel method and a system to measure the OMF region and derive the surgical measurement from the mapping. The process is named as "Landmarks method".

Landmarks are a series of points placed on various locations of the subject and the though software pointer calculations measure the distances and angles between them. This provides a clear tool to measure distances both in 2D and 3D as the need may be.

In this method landmarks were placed along the condyle, coronoid process, ramus and mandible sections. Various sections of the lower jaw are as labelled in below in the figure 13. The landmarks are mirrored on both the sides of the skull and on both the scans of the dataset. The landmarks are as shown in the figure 14.

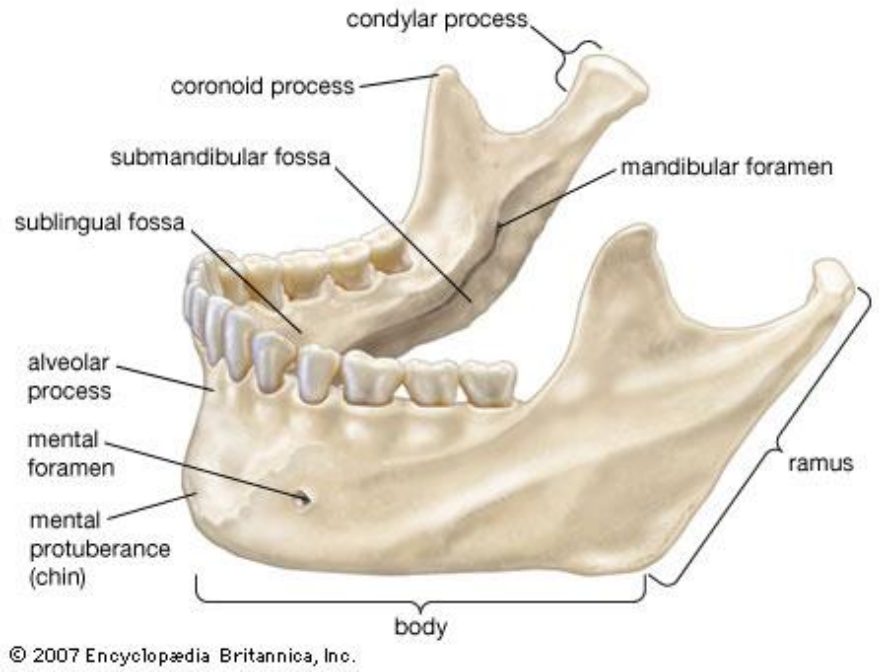

Figure 13: Anatomy of the lower Jaw.

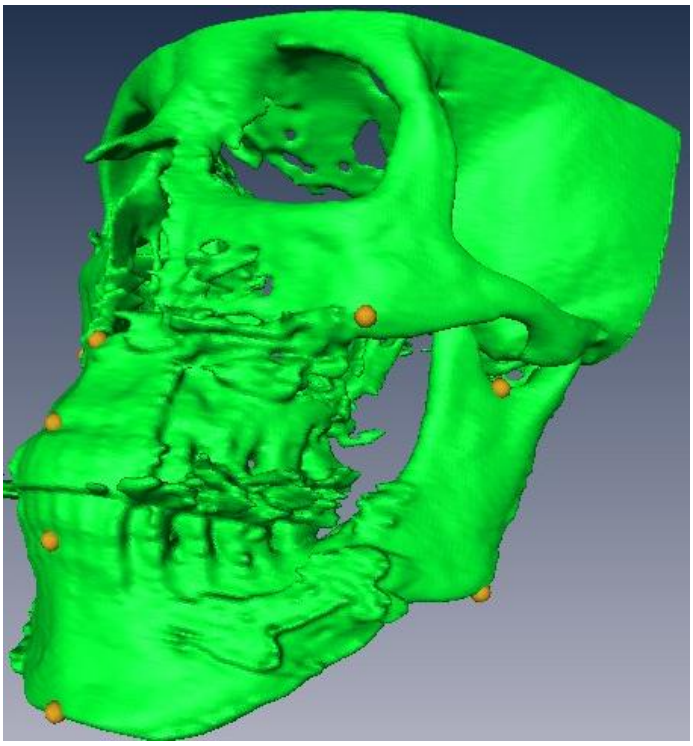

Figure 14: Landmarks placement on the various sections of the segmented 3D volume. Landmarks are shown in golden points.

Landmarks after placement on the various sections remain stationary when the 3D models are rotated or translated in their corresponding axis. The landmarks can be altered if needed. Landmarks placement and its location selection can be varied depending on the type of the orthodontic surgery. Usually either of the jaw or both the jaws undergo surgery and hence placement of landmarks can be skilfully adapted in this technique.

The measurement tool is used to calculate the inter-landmarks tool. An example used in the inter-landmarks mapping is shown in the figure 15. Mapping can be adapted according to surgery type.

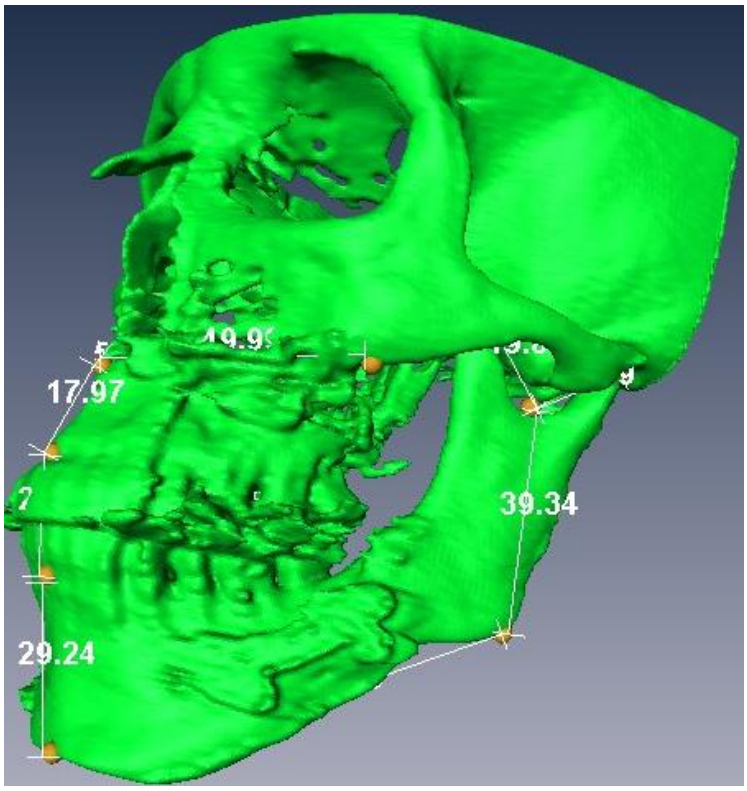

Figure 15: Landmarks points with mapping structure to capture both upper jaw and lower jaw measurements

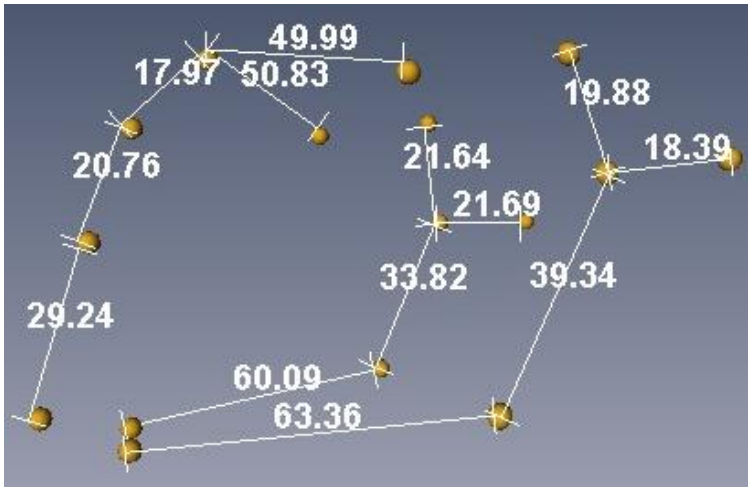

Figure 16: Mapping structure without the segmented 3D volume data.

Inter-landmarks are calculated and tabulated for both presurgery and postsurgery models. The differences in the postsurgery with presurgery as reference provide the surgery change information. The differences can be computed for both inter-landmarks distances and angles. This provides 3D perspective of the change. An example of this process is discussed in detail in the next section under the results heading. Figure 16 shows the landmarks mapping without the 3D data, this provides a clearer view of the inter-landmark distances and mapping structure thus providing a feedback to correct the distance lengths in case if it is out of bounds.

The resolution of the spheres of the landmarks can be improved by changing the size by moving the slider in the user interface. However care should be taken that when comparing the inter-landmark distances in the datasets, the size of the spheres are set same or chosen as default.

The landmarks method was one of the approaches taken to assess the geometry of the jaws. This method still requires some scientific standardization but serves the purpose of the objective of the thesis work. No previous documentation in the measurement standards similar to EEG's 10-20 system was found.

5. RESULTS

5.1 Segmentation analysis

The sequential datasets were registered using the rigid mutual information type in the affine registration module. The 3D volumes were cropped and aligned to focus on the region of interest. Segmentation was performed selecting the appropriate intensities highlighting the bony structures. This step eliminates extraneous feature of the CBCT volume such as chin plate, spinal cord and posterior skull.

Rigid mutual information is a concept carried over from information theory which measures the statistical dependencies of two variables or the quantity of information each variable contains about another [31]. Due to rigid type of registration the datasets are not scaled in the registration and superimposition process which would otherwise mean that dimensions of the datasets are compromised.

Segmentation in this method requires initial manual selection of the intensities. But once the segmentation seeds are appropriately placed in certain regions the 3D replication to all the 3D slices are automatically done in real time. This real time volume rendering allows adjusting the segmentation window and control region of growing.

The segmentation of the skull and different view of the region of interest is as shown the figure 17. The process of segmentation is similar in both the scans of the dataset. The colour of the segmentation 3D volume is different between in the scans to enable visually distinction. As a general rule the green coloured 3D volume represents presurgery model and red coloured 3D volume represents postsurgery model. The segmentation as illustrated in the models in following diagram is not usually complete and some sections of the 3D model are missing. This is due to presence of extraneous noise or absence of data in those sections of the scans from the imaging equipment.

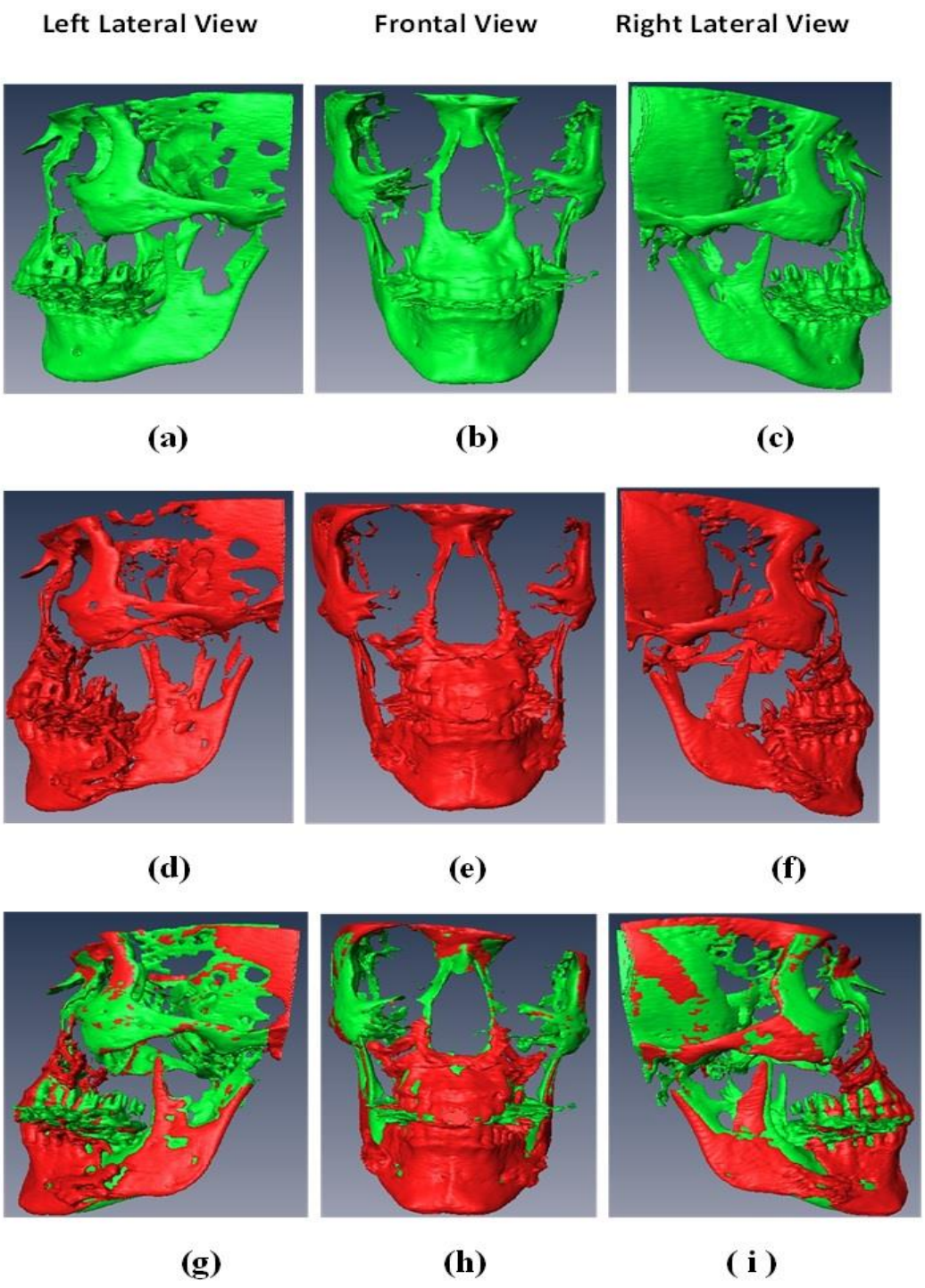

Figure 17: The above figure shown segmentation view for presurgery scans (a, b, c), postsurgery (d, e, f) and superimposed scans (g, h, i). Some sections of the scans are missing showing the limitations of the segmentation process.

Segmentation can differ amongst users and different adopted practices. An analysis of inter-user variations was simulated by performing the segmentation twice in different sittings. Then surface distance analysis was performed to analyse the differences. The table 1 below shows the statistical analysis of the task.

Mean (mm)	Deviation(mm)	RMS(mm)	Max(mm)	Median(mm)	Above Threshold
0.1	0.5	0.5	18.4	0.04	1.6

Table 1: Statistical information indicating inter-user differences for segmentation

The surface analysis for inter-user example is as shown in figure 18 below. The table above shows statistical information for the 3D model shown in the figure below. This translates simply that if the users are trained the differences in the end results could range from minimum to negligible.

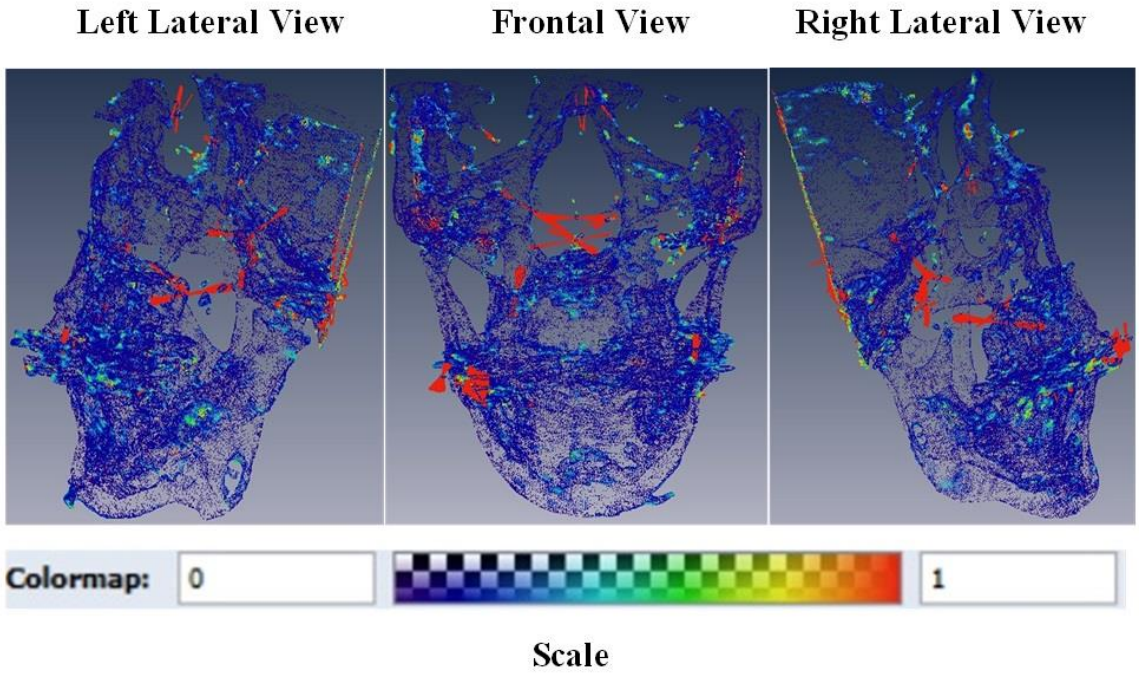

Figure 18: Surface distance 3D models illustrating the inter-user differences in segmentation. The map primarily consists of blue vector arrows indicating minimum surface distance or differences between the segmented models.

5.2 Superimposition analysis

Affine registration technique superimposes the sequential dataset. The surface distance between the superimposed models can be calculated. The superposition is performed on different subjects with different types of surgery. The figure 19 illustrates the surface distance mesh for one of the surgery type. AMIRA provides a good tool in the surface-distance module for visually and statically analysing the superimposition via surface distances measures.

The surface distance is calculated as the closest distance between two triangulated surfaces. Once the segmentation of the datasets is calculated, the surfaces upon volume rendering are automatically triangulated with tetrahedron meshes. So the surfaces at the end of the segmentation results in surfaces with tetrahedron structures. Hence surface distance and its mapping are easily quantifiable.

The surface distance apart from the statistical measures can visualised in the form of points or vectors. In the example that follows vector analysis has been implemented. Vector analysis carries information about the direction and magnitude as a result the output can be colour coded.

The superimposed images can be statistically analysed as shown in the table 2 below.

Mean (mm)	Deviation(mm)	RMS(mm)	Max(mm)	Median(mm)	Above Threshold
1.3	1.5	2.0	12.0	0.07	60.9

Table 2: Superimposition statistical information for the dataset shown in figure 19

The information in table 2 pertains to statistical analysis of the tetrahedron surface computations. So the maximum deviation in this case is 12 mm. But the data does not provide information about the actual sections which caused these statistical measures. However the vector analysis provides the missing information about the location, direction and magnitude. This is illustrated in figure 19.

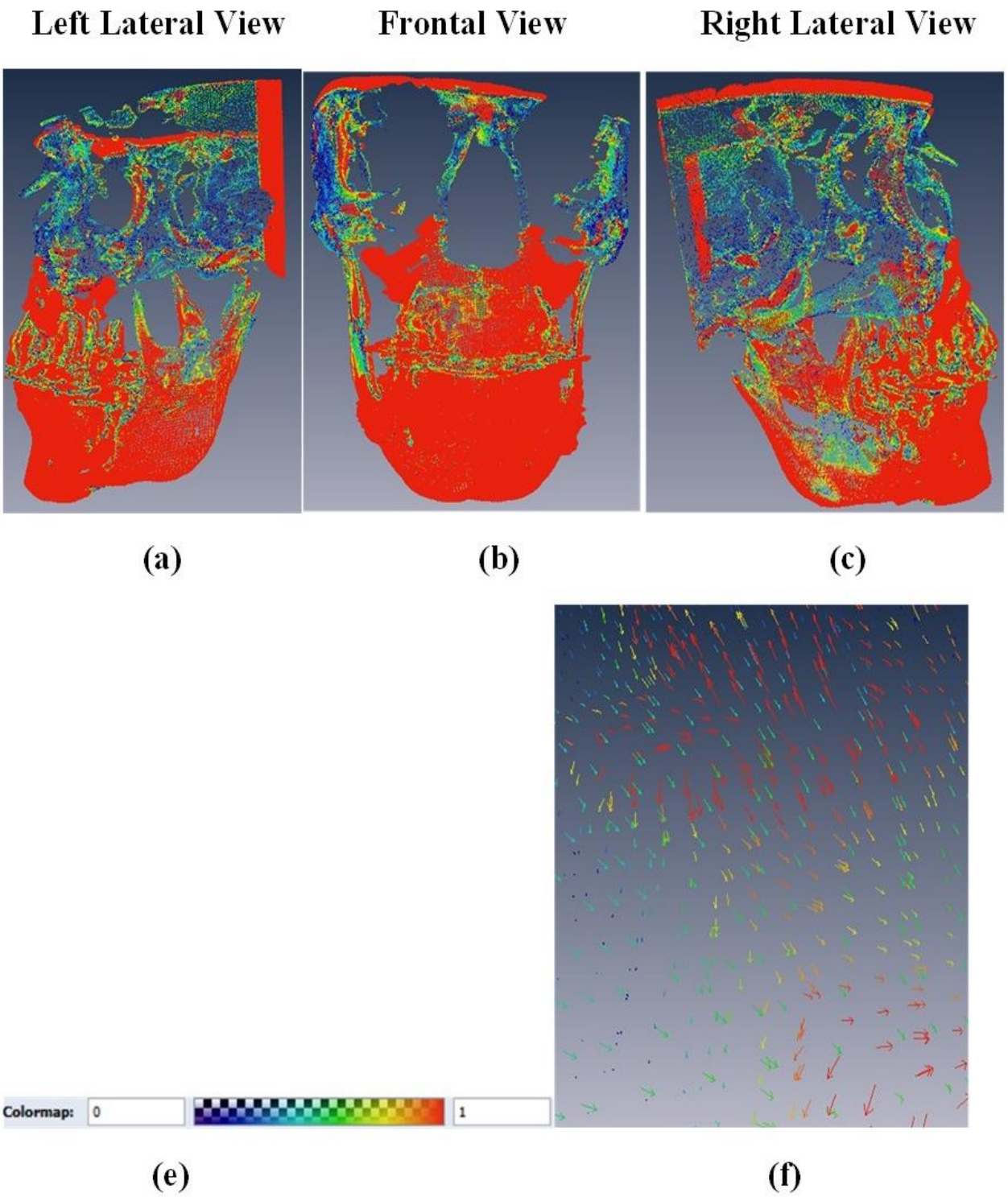

Figure 19: Surface distance measure analysis. The models are made of vectors pointing the direction of change in the surface distance with respect to presurgery model. The scale is as given in (e) and the zoomed in version is seen in figure (f).

5.3 Geometrical calculations analysis

The geometrical calculations were done using the Measurement module in AMIRA software. The module provides the ability to measure two-dimensional and three-dimensional distances and angles.

The application of the method relies on the selecting the points of measurement in the measurement module. The process of selecting the series of points can be termed as mapping. Mapping of the various distances depends on the type of surgery and can hence be altered. The figure 20 below shows an example of mapping of the skull to assess its geometry.

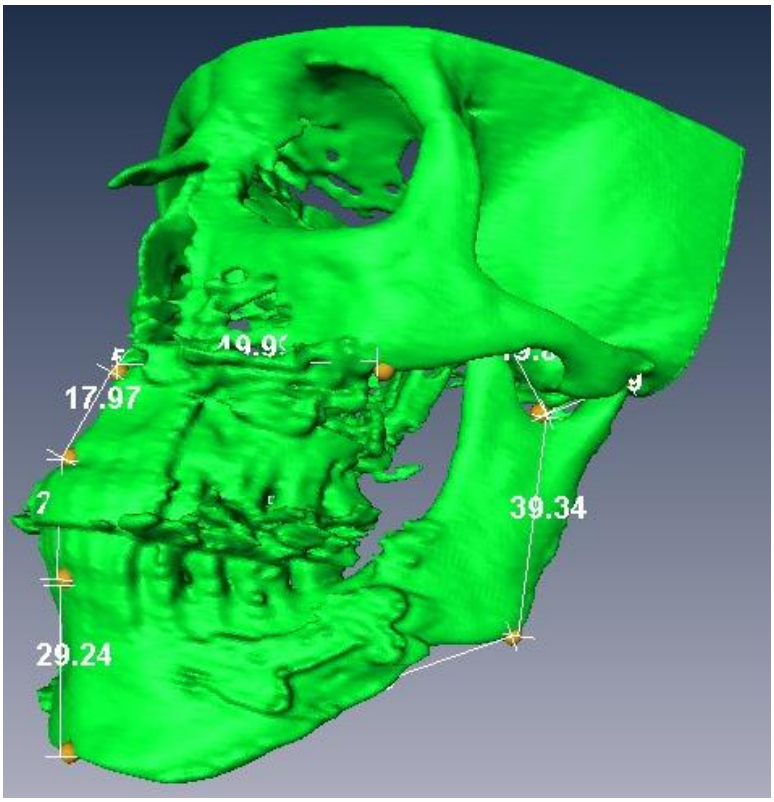

Figure 20: Example of mapping of the skull with landmarks and various inter-landmark distances.

After a certain geometry mapping is selected, landmarks were placed on the various sections of the 3D volumes. The selection of the landmark points provides enough flexibility and reliability in the 3D measurements. The landmarks sizes, colour can be changed to improve the accuracy and positional requirements. Once the landmarks are placed inter-landmarks distance can be measured. Figure 21 shows the inter-landmark distances for a chosen geometry mapping.

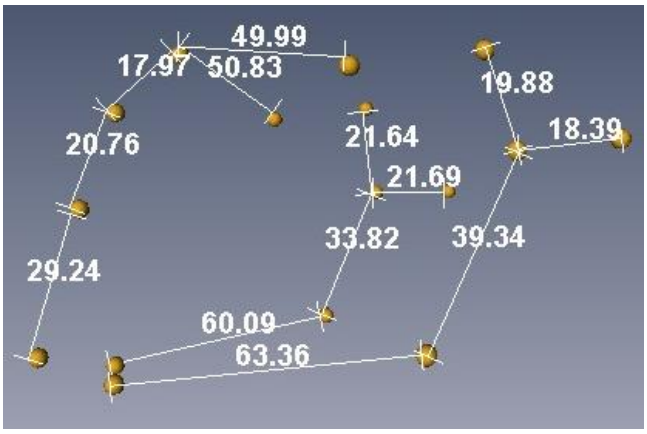

Figure 21: The mapping skeleton of the skull without the 3D model.

5.4 Surgery change estimation analysis

The orthodontics surgery involves relocating either of the jaw or both as per subject's requirement. The landmarks and its inter-landmark distances provide a good estimation of the surgery change three-dimensionally. The inter-landmarks distances of the presurgery and postsurgery dataset are compared and change due to the orthognathic surgery can be analysed.

The table 3 represents the change estimation analysis for lower jaw and upper jaw type of surgery. The figure 22 shows the sample measurement data with mapping. This data is further analysed in table 3.

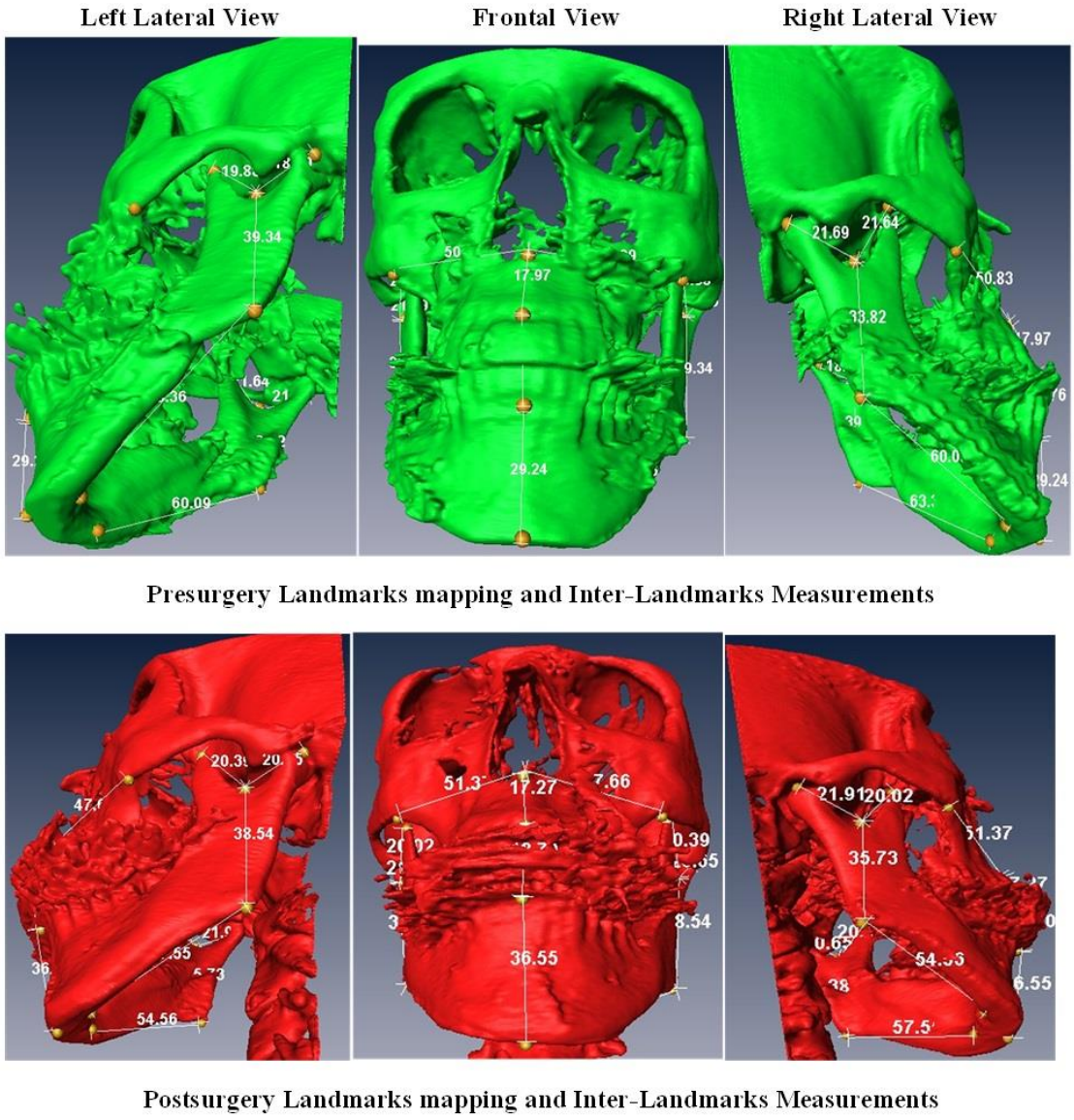

Figure 22: Sample data with mapping on Presurgery and Postsurgery 3D model.

Section of the Skull	Presurgery Measurement (x) (mm)	Postsurgery Measurement (y) (mm)	Difference (x) - (y) (mm)	Difference in percentage ((x-y)/(x)* 100 (%)
Left Lateral View				
Condyle	21.9	21.7	-0.2	-1.0
Coronoid process	20.0	21.6	1.6	8.0
Ramus	35.7	33.8	-1.9	-5.3
Frontal Section				
Maxilla	18.7	20.8	2.0	11.0
Mandible	36.5	29.2	-7.3	-20
Right Lateral View				
Condyle	20.4	19.9	-0.5	-2.5
Coronoid process	20.6	18.4	-2.2	-10.9
Ramus	38.5	39.3	0.8	2.07

Table 3: Assessment of the surgical changes utilizing the data from the models as shown in the previous figure is illustrated. The table shows the difference in lengths in various sections of the skull. For simplicity only distance measurements are considered.

5.5 Calibration and Validation of measurements

The landmarks method provides a fine technique to measure the various lengths of the CBCT scan. To validate the measurement legitimacy phantom CT scans from General Electric website was used. The figure 23 below shows the phantom outline used in the validation process.

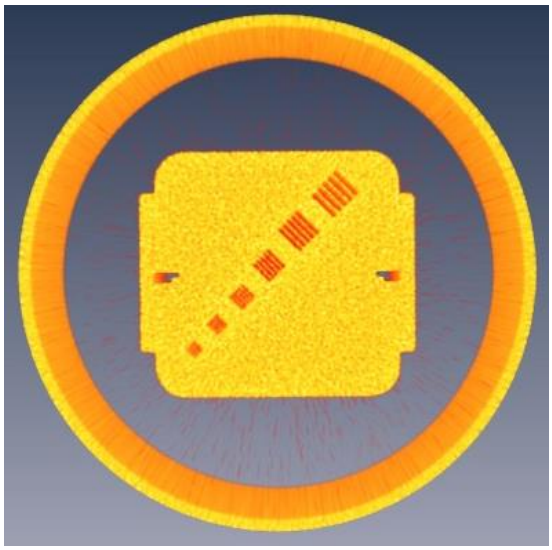

Figure 23: Phantom model used for testing the measurements

The phantom had standard straight and curved edges. The actual dimensions of the phantom were unknown. To validate the measurements however IMAGEJ software was used as a comparison. ImageJ has been widely used in image processing algorithms and it has been widely accepted in the scientific community. The phantom was thus comparatively measured in both AMIRA's landmark method and ImageJ's measurement tool. Table below provides statistical data of the two software measurements.

Serial No.	Measuring Surface	ImageJ Soft-ware (mm)	Amira (mm)	Devia-tion from ImageJ (mm)	Percentage of deviation (%)
1	Diameter of the outermost ring	214.0	213.4	0.6	0.3
2	thickness of the Ring	5.7	4.6	1.1	20.5
3	Inner diagonal square edge to square edge 1	129.3	128.9	0.3	0.3
4	Inner diagonal square edge to square edge 2	128.2	128.4	-0.2	-0.1
5	Inner diagonal curved edge to curved edge 1	132.8	132.6	0.2	0.1
6	Inner diagonal curved edge to curved edge 2	133.4	132.0	1.4	1.04
7	Length of the square edge1	65.9	65.3	0.6	0.9
8	Length of the square edge2	65.6	65.1	0.5	0.8

Table 4: Statistical analysis of the measurements between ImageJ and AMIRA

The data from above table shows that the measurements are very close to standard software used in research purposes. There are a few considerations in the above validation experiment. Firstly, the data used for validation was from a CT scan of high resolution to provide clear measurements. Secondly the measurements in the ImageJ were performed on the scanned data itself and not on the segmented 3D model. While on other hand the scan was segmented and landmark method was used in measurements in AMIRA software. Next, the distances to measured and edges were randomly taken but along regular surfaces.

Analyzing the above data shows that despite losing some advantage over the ImageJ software due to additional segmentation step added, the method used with AMIRA's process excelled in the measurements, which were in the acceptable range with negligible deviations.

The qualities of the datasets however vary from imaging equipment to imaging equipment. The step of calibration involved adjusting the values measured after performing validation steps locally and prior to analysis. However in the validation step it is recommended to use CBCT datasets of known dimension rather employing comparison technique as used in this section of the experiment.

The accuracy of the measurements can be further improved by calibrating the measurements through mathematical alterations as per the local condition needs and adapted to

the imaging equipment [32]. But as per the developers of AMIRA the software is to be used for research and assessment tool and not as a standalone medical device.

6. DISCUSSION

The CBCT imaging has been very popular in the orthodontics field and its technological advancement cannot be ignored. But the methods to analyse the data and interpret the results have however lagged. The orthodontics department of the Tampere University Hospital identified the need to have a method or a tool to measure the CBCT scans in 3D. The method in discussion aims to fulfil the gap identified in the analysis of acquired CBCT datasets.

6.1 Anonymized data

Though the CBCT is quite frequently used in Tampere University Hospital, procurement of imaging data was not a simple task. The dataset had to be uniformly acquired in similar field of view, resolution and contrast. The initial datasets acquired were quite random and acquired in different settings. This added complexities due to mismatch in imaging equipment and hence mismatch in size and resolution of the scans. These datasets ideally cannot be compared in the method discussed without resampling and may even require interpolation of image stacks. So in the method development stage these mismatched datasets were altogether eliminated.

The next datasets were acquired with a set of preconditions. The image datasets were acquired in same imaging equipment and similar acquisitions settings. This condition results in datasets of comparable resolution, contrast and axis alignment of 3D images.

The dataset included two sets of scans. The first scan was performed prior to scheduled orthognathic surgery with both jaws in closed position. The second scan was performed after the surgery in four weeks with closed jaw position. The datasets were of 0.4mm voxels size with 575x575x575 dimensions.

CBCT scans involve significant radiation exposure for adequate resolution and contrast. The significance of CBCT scans w.r.t to radiation exposure is still questionable. So ideally CBCT scans are not used if surgery is not involved. The subjects may not even undergo a follow-up scan after surgery. So the datasets can be quite rare with set preconditions. As, improvements in CBCT technology continues there are chances of decrease in radiation dose in the future.

6.2 Processing of collected data

CBCT data involves scans in 3D. Volume rendering and 3D volume processing requires high computational processors with high end graphics. But due to advances in computer processors and standalone graphic technology, hardware is quite affordable and widely available.

Reformatting and resizing CBCT scans are very computationally demanding. So the preconditions in selecting the datasets eliminate this problem. The visual display of CBCT volumes is rather simple and does not require high end processors. But since the task involves processing of 3D volumes, a workstation with high end graphics was used.

6.3 Segmentation of 3D volumes

Segmentation by extracting only a certain region of interest and volume rendering is not without its challenges. The presence of metallic implant in the subject's scan can compromise the segmentation to a certain extent due presence of noisy intensities. In the method under discussion the segmentation to begin with involves selection of certain grey scale intensities and labelling it. The selected intensity and the segmentation window size are done manually.

In CBCT scans there is almost uniform intensity level for jaw bones and skull. Hence extraneous features are easily removed. Due to this the segmentation process can be repeated with similar results. The inter-user differences amongst trained users will be minimized because the initial parameter selection is very few. The volume rendering if reflected in 3D almost instantly with the ability to make real time adjustments. The noise levels and the region of segmentation all can be adjusted before finalizing the segmentation model.

However the segmentation models tend to have noisy features where the upper and lower jaws meet. But the noisy projection does not alter the geometry mapping or landmarks measurement methods. These projections are as shown in the figure 24.

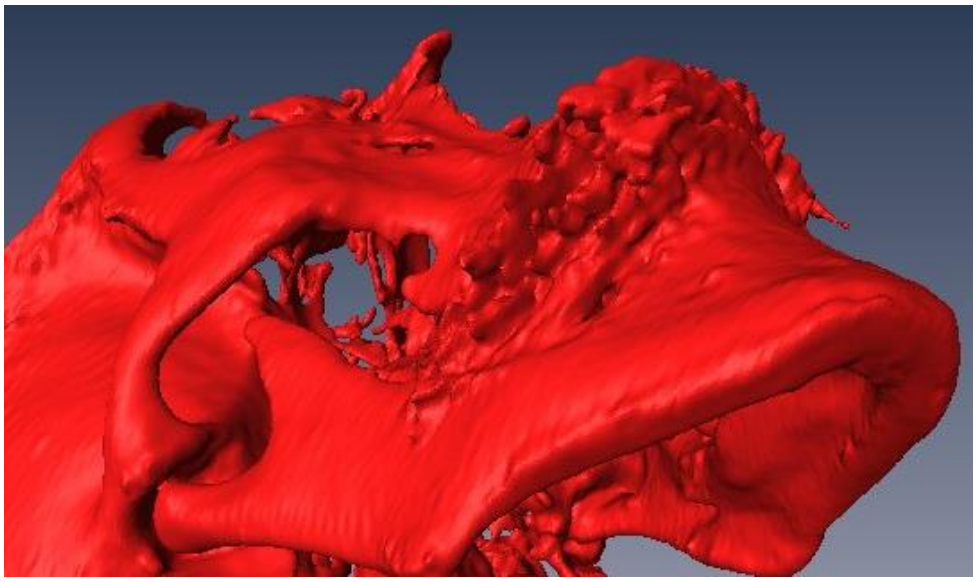

Figure 24: Noisy projections at the intersections of the upper and lower jaw.

The segmented model of the postsurgery reveals visual information of the surgery change, the gaps introduced and attachment of supporting splints, figure 23 shows the features mentioned.

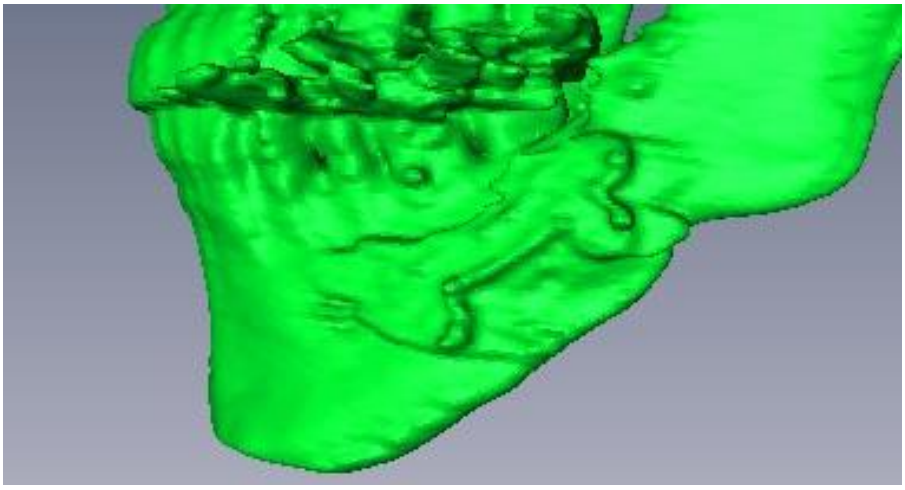

Figure 25: The surgery change markers and splint imprints visible in the segmented models of the postsurgery scans.

The segmentation process could be greatly improved and automated if fully automated segmentation module is present; however such a tool is not yet integrated. On the other hand if the scans were of high quality the segmentation can be improved greatly but this means unwanted higher radiation dosage to patients, not an ideal situation.

6.4 Geometrical calculations

The geometrical calculations are primarily dependent on the mapping of the jaw and other related skull structures. At the basic the method is applicable to measure any geometry of the CBCT scanned volumes. In this application however the measurements have been focussed to get the details of the jaws of the subjects.

The CBCT scans are initially cropped to eliminate other anatomies such as spinal cord, back spherical half of the skull and forehead. So prior to mapping the region of interest is already focussed to suit the dental application. The geometrical mapping is designed to extract the information which reflects the changes in the jaw structure.

The mapping of the landmark points can be customised according to the orthognathic surgery. If only lower jaw has been surgically altered landmark points to highlight this change can be focused and extra point from the upper can be eliminated. The process is similar in case of upper jaw operation. The complexities in the geometries increases when both the jaws are altered, the points are to be strategically chosen at the discretion of the practitioner to capture the overall changes.

The landmarks points and placements options are provided as a separate module in AMIRA software. The size and colour of the landmark points can be altered. The module provides easy user interface for altering the landmarks. One of the features of landmarks is that the landmarks skeleton in two scans in dataset can be superimposed to get first-hand information of the surgical change before the distances are measures. The figure 26 below shows this ability in which the landmarks are superimposed.

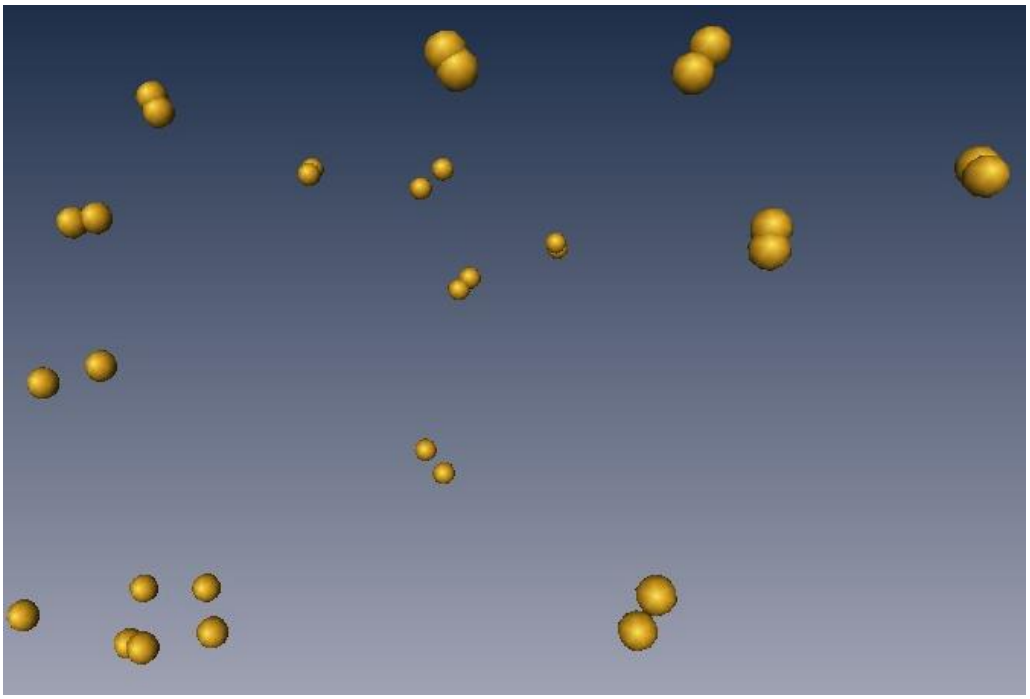

Figure 26: Landmarks from the dataset scans, some points in the upper section are closer than the lower section where there is definte change in the position. This also depicts the ability to superimpose the landmarks before the actual measurement is done.

The measurement module provides multiple options of measurements. The distances can be measured in both 2D and 3D, same applies for angle measurement. The measurement is simple task once the landmarks are already mapped on the region of interest. This task would can tricky without the landmarks to demark the ending of the measurand. The landmarks module and the measurement module together provide a neat way to measure the geometry of the region of interest. Figure 27 shows an example of the final result of calculating the distances after the mapping is done.

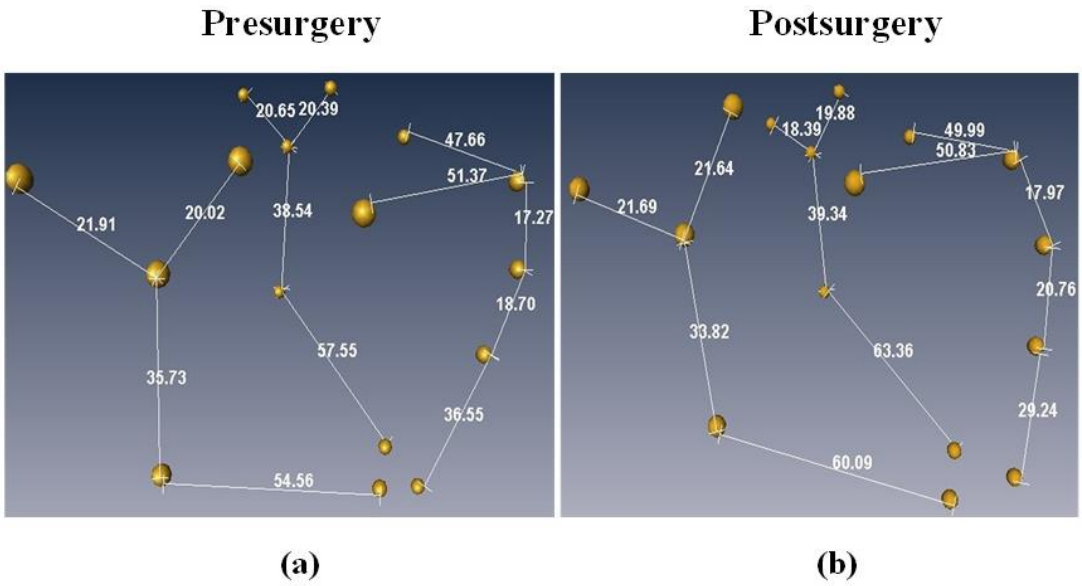

Figure 27: Inter-Landmarks mapping from Presurgery and Postsurgery models.

6.5 Accuracy and limitations

The method's overall accuracy depends on the crucial superimposition step. This has been shown to have sub-voxel accuracy in the surface distance tests as illustrated in table 5.

Subject	Mean (mm)	Deviation(mm)	RMS(mm)	Max(mm)	Median(mm)
1	1.3	1.5	1.9	12.9	0.78
2	1.3	1.5	2.0	12.0	0.7
3	1.2	1.5	1.9	10.3	0.6

Table 5: Surface distances for different subjects showing sub-voxel accuracies

As shown in the above table the mean distances are within 1.3mm and other parameters are very close.

The segmentation step involves significant user input and hence accuracy can depend on the user's experience and overall understanding of the process, however is still questionable. But as shown in table 1, inter-user difference is under acceptable levels and hence the overall accuracy can still be controlled. The study was done with CBCT scans in 0.4mm voxel size and level of error was minimal. The segmentation step could be improved if the resolution and contrast of the CBCT scan could be significantly improved, but this at the current stage means more undesired radiation dosage on the sub-

jects, which is unlikely. Also if the segmentation process is fully automated the user introduced errors can be eliminated altogether.

The CBCT scans of fully grown adults would be ideal when scans are compared after certain duration. Other algorithms such as Elastic registration can provide more accuracy but are currently computationally demanding.

6.6 Methodology summary

The overall process followed in the thesis can be visually summarized as shown in the figure 28.

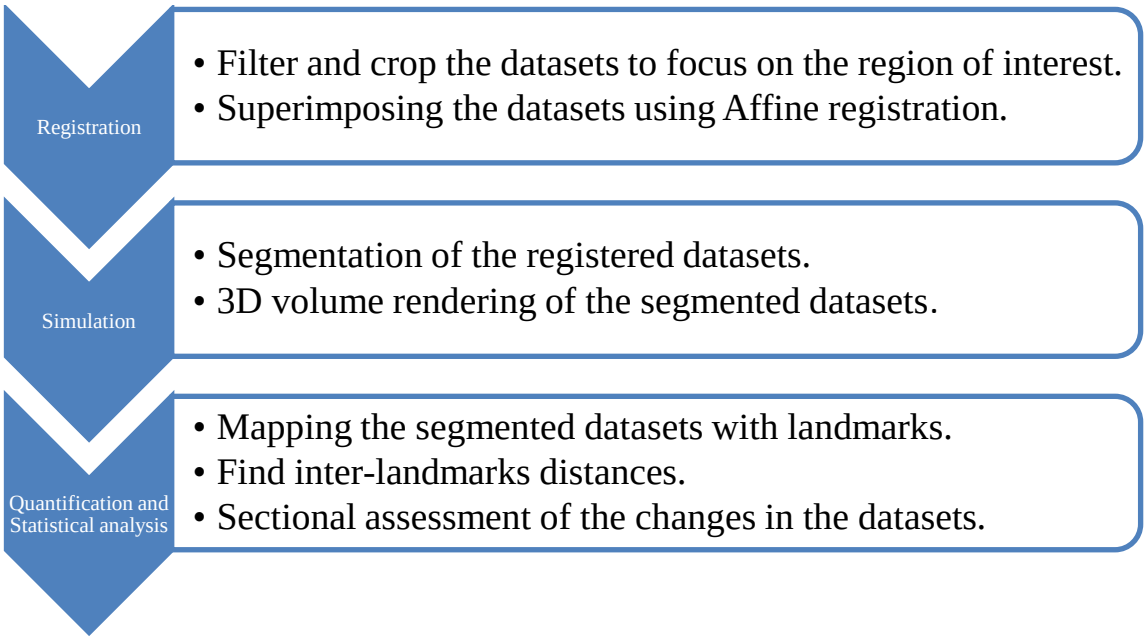

Figure 28: Essential steps in the method used to find the geometry of the CBCT scans.

The steps of registration, simulations and quantification summarize the essential steps discussed in the thesis. The first two steps are widely discussed in the medical imaging research areas. However the last step of quantification and statistical analysis method is quite novel and previous usage of the "Landmarks method" was not found.

6.7 Scope for future improvements

The method discussed is just one of the tools to complement the advances in CBCT technologies. The method can easily be applied to 3D scans of other areas of the human body. The limitation of the areas of comparison and superposition is only limited to computational limits of the rigid registration and hardware capabilities.

The overall methodology can be developed using open source platform thus avoiding cost incurred in yearly license procurement for commercially available software such as AMIRA software. But this would entail significant research cost in the software development from scratch. But once developed the tool can be distributed freely and upgraded with minimum operating costs.

7. CONCLUSION

The efforts in this thesis primarily focussed on developing the a streamlined method for CBCT scans volume rendering, superposition of datasets and its geometry measurements in an integrated software which is well documented and well supported. This methodology and technique is documented in guidance manual in steps, in a user-friendly fashion requiring minimum technical know-how. Agreed the steps consume time initially but it achieves the set objectives with high quality output. The following set objectives were comprehensively achieved:

1. A reproducible method of volume rendering, superposition in easy to follow steps.
2. The accuracy of the method in superposition of datasets.
3. Geometrical mapping of the segmented 3D volume.
4. Novel method called “Landmarks method” for measuring the 3D volumes and estimating the surgery change
5. Laying the ground work for similar tools for the future or design for dedicated open-source tools.

REFERENCES

1. *What is Cone-Beam CT and How Does it Work?* **Scarfe, William C and Farman, Allan G.** 2008, The Dental Clinics of North America, Vol. 52, pp. 707-730.

2. *Generation of continuous and pulsed diagnostic imaging x-ray radiation using a carbon-nanotube-based field-emission cathode.* **G.Z, Yue, et al.** 2, 2002, American Institute of Physics, Vol. 81.

3. **J.D.Bronzino.** X-Ray. [ed.] CRC Press. *Biomedical Engineering Handbook.* Second. s.l. : CRC Press LLC, 2000.

4. High-Performance Data-Acquisition System Enhances Images for Digital X-Ray and MRI. *http://www.analog.com/.* [Online] October 2013. [Cited: March 2, 2014.] http://www.analog.com/library/analogdialogue/archives/47-10/digital_xray.html.

5. *X-ray computed tomography.* **Kalender, Willi A.** Phys. Med. Biol. 51 (2006) R29–R43, 2006, INSTITUTE OF PHYSICS PUBLISHING.

6. *X-ray CT: An engineering synthesis of multiscientific principles.* **RA, Robb .** 1982, CRC Crit Rev Biomed Eng 7, pp. 265–334.

7. *Cone-beam computerized tomography (CBCT) imaging of the oral and maxillofacial region: A systematic review of the literature.* **Vos, W. De, Casselman, J. and Swennen, G. R. J.** Bruges, Belgium : International Association of Oral and Maxillofacial Surgeons, 2009, Vols. 0901-5027/060609.

8. *Reliability and accuracy of cone-beam computed tomography dental measurements.* **Baumgaertel, Sebastian, et al.** Cleveland, Ohio : Am J Orthod Dentofacial Orthop, 2007, Vols. 136:19-28.

9. *Cone-beam computerized tomography (CBCT) imaging of the oral and maxillofacial region: A systematic review of the literature.* **Vos, W. De and Casselman, J.** 2009, Int. J. Oral Maxillofac. Surg, Vols. 609-625, p. 38.

10. **Theese, Courtney.** Concept-CBCT-Scanner. *http://cargocollective.com/.* [Online] NA 2014. [Cited: March 4, 2015.] http://cargocollective.com/courtneytheese/Concept-CBCT-Scanner.

11. *Reduction of artifacts in dental cone beam CT images to improve the three dimensional image reconstruction improve the three dimensional image reconstruction.* **Ibraheem, Issa.** Damascus, Syria : JBiSE J. Biomedical Science and Engineering, 2011, Vols. 5, 409-415.

12. *Cone-Beam Computed Tomography in Orthodontics: Benefits and Limitations.* **Holberg, Christof, et al.** s.l. : Journal of Orofacial Orthopedics, 2005, Vols. 66:434–44.

13. *The influence of partial volume averaging on sphere detectability in computed tomography.* **Dean, P.B and D.B, Plewes.** 01, United Kingdom : Physics in Medicine and Biology, 1981, Vol. 13.

14. *Three-dimensional accuracy of measurements made with software on cone-beam computed tomography images.* **Lagravère, Manuel O, et al.** 2008, Am J Orthod Dentofacial Orthop, Vols. 34:112-16.

15. *Linear Accuracy and Reliability of Cone Beam CT Derived 3-Dimensional Images Constructed Using an Orthodontic Volumetric Rendering Program.* **Periago, Danielle R. , et al.**

16. *Accuracy of linear measurements using dental cone beam and conventional multislice computed tomography.* **Suomalainen, A, et al.** 2008, Dentomaxillofacial Radiology, Vols. 37, 10–17.

17. *Analysis of the accuracy of linear measurements obtained by cone beam computed tomography (CBCT-NewTom).* **Lascala, CA, Panella, J and Marques, MM.** s.l. : Dentomaxillofacial Radiology, 2003, Vol. 0.1259/dmfr/25500850.

18. *Accuracy and reliability of craniometric measurements on lateral cephalometry and 3D measurements on CBCT scans.* **Gribel, Bruno Fraza˜o , et al.** s.l. : The EH Angle Education and Research Foundation, 2010, Vols. Vol 81, No 1, 2011.

19. *Digital image smoothing and the sigma filter.* **Lee, Jong-Sen.** 2, 1983, Elsevier Inc, Vol. 24, p. 14.

20. *Three-Dimensional Treatment Planning of Orthognathic Surgery in the Era of Virtual Imaging.* **R.J. Swennen, Gwen and Mollemans, Wouter.** 2009, American Association of Oral and Maxillofacial Surgeons, Vols. 67:2080-2092.

21. *User-guided 3D active contour segmentation of anatomical structures: Significantly improved efficiency and reliability.* **Yushkevich, Paul A., et al.** 2006, Elsevier Inc., Vols. NeuroImage 31 (2006) 1116 – 1128.

22. *Superimposition of 3D cone-beam CT models in orthognathic surgery.* **Simões da Motta, Alexandre Trindade , et al.** s.l. : Dental Press J. Orthod., 2010, Vols. v. 15, no. 2, p. 39-41,.

23. *Image registration methods: a survey.* **Zitova, Barbara and Flusser, Jan.** 2003, Elsevier B.V, Vols. 0262-8856/03.

24. *Three-dimensional surgical simulation.* **Cevidanes, Lucia H. C., et al.** 138:361-71, 2010, Am J Orthod Dentofacial Orthop, TECHNO BYTES.

25. Corrective Jaw Surgery - Orthognathic Surgery. *http://www.cosurgicalarts.com/.* [Online] [Cited: March 2, 2015.] http://www.cosurgicalarts.com/corrective_jaw_surgery.php.

26. *The skeletal stability of one-piece Le Fort 1 osteotomy to advance the maxilla Part 1. Stability resultingfrom non-bone grafted rigid fixation.* **Hoffman, G.R. and Brennan, P.A.** s.l. : British Journal of Oral and Maxillofacial Surgery, 2004, Vols. 42, 221—225.

27. *High-Accuracy 3D Image-Based Registration of Endoscopic Video to C-Arm Cone-Beam CT for Image-Guided Skull Base Surgery.* **Mirota, Daniel J, et al.** s.l. : SPIE Medical Imaging, 2011, Vol. 7964.

28. *A comparison between 2D and 3D cephalometry on CBCT scans of human skulls.* **van Vlijmen, O. J. C., et al.** s.l. : Int. J. Oral Maxillofac. Surg, 2010, Vols. 39: 156–160.

29. *Reliability and accuracy of cone-beam computed tomography dental measurements.* **Baumgaertel, Sebastian, et al.** Cleveland, Ohio : Am J Orthod Dentofacial Orthop, 2009, Vols. 136:19-28.

30. Features- Planmeca-ProMax-3D-Max. *http://www.planmeca.com/.* [Online] 2015. [Cited: March 2, 2015.] http://www.planmeca.com/na/Imaging/3D-imaging---Key-features/Planmeca-ProMax-3D-Max/.

31. *Multimodality Image Registration by Maximization of Mutual Information.* **Frederik, Maes, et al.** 2, 1998, IEEE TRANSACTIONS ON MEDICAL IMAGING, Vol. 16.

32. *Accuracy of three-dimensional measurements obtained from cone beam computed tomography surface-rendered images for cephalometric analysis: infl uence of patient scanning position.* **Hassan, Bassam, van der Stelt, Paul and Sanderink, Gerard.** Amsterdam (ACTA), The Netherlands : Oxford University Press on behalf of the European Orthodontic Society, 2008.

APPENDIX A: AMIRA APPLICATION GUIDE

1. Loading image datasets

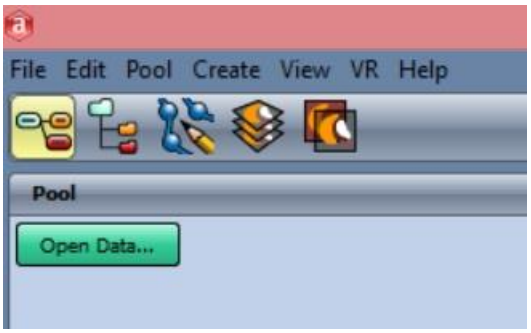

- Click on “Open Data” and navigate to the file location.

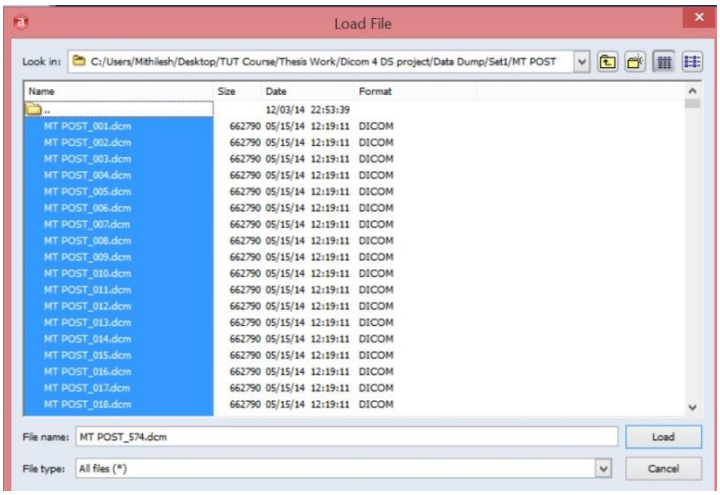

- Select all the dicom files.

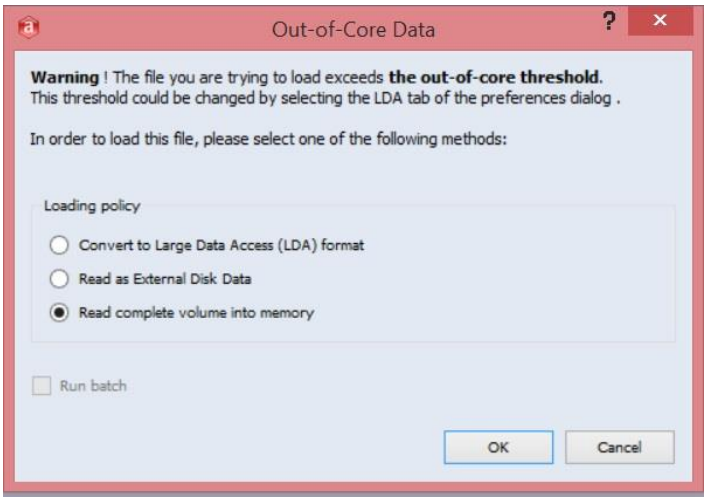

- Choose the 3rd option from loading policy

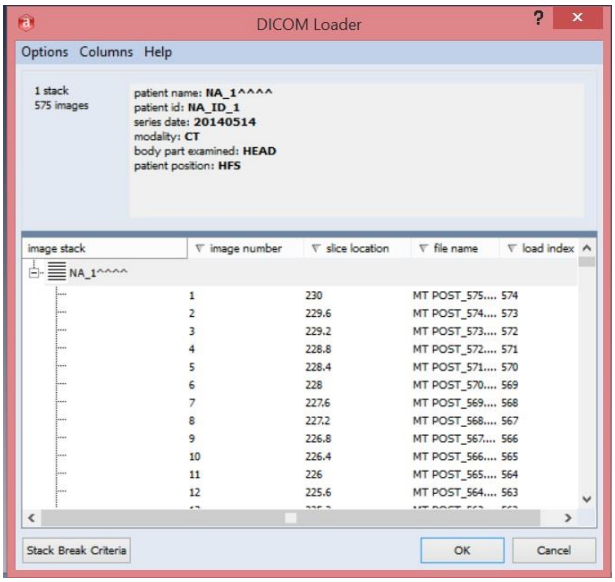

- Click on “OK” after reading the header info.

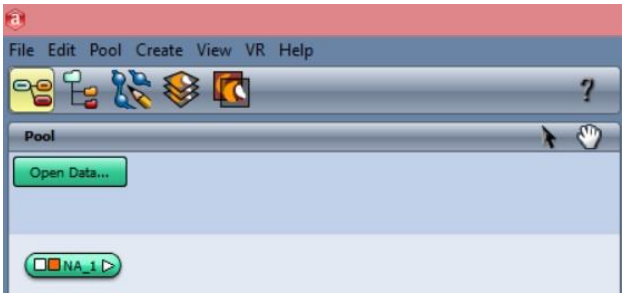

- Once the file is loaded a data segment named “NA_1” will be created.

- Rename by pressing “F2” after selecting the box and name it.
- Data loaded can be visualized by clicking “Volren” button.

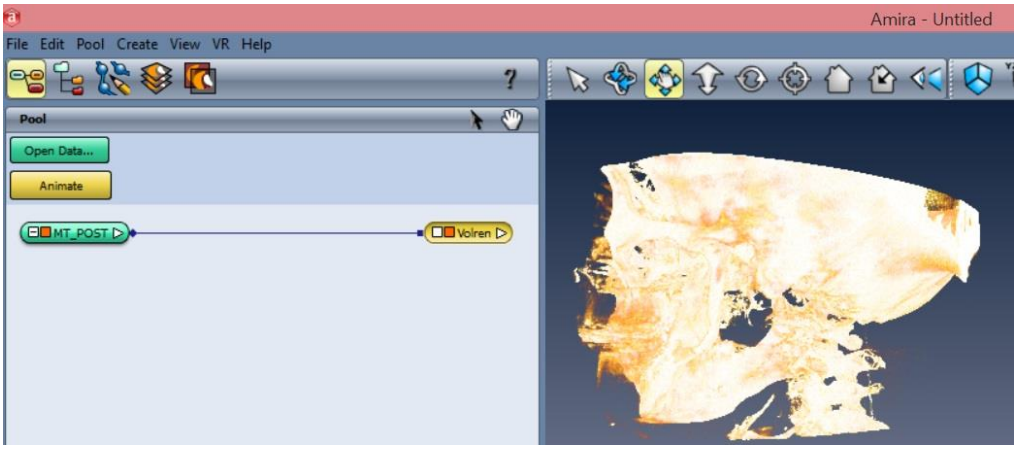

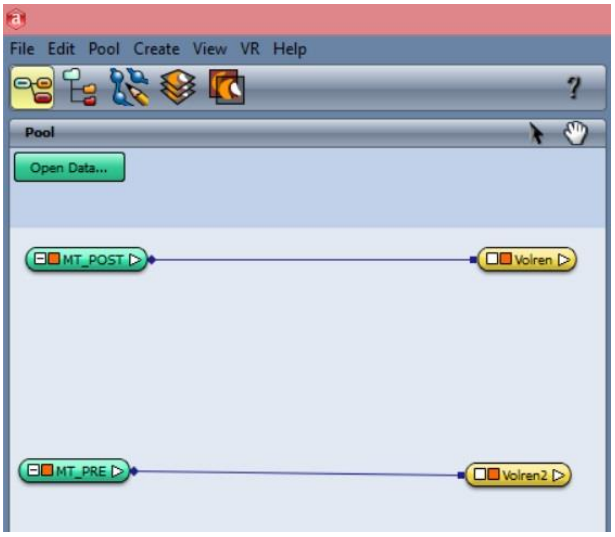

- Repeat the process for next scan too. At this step there should be two data items. Example: “ MT_PRE” and “MT_POST”
- Under “File” save the network and data”

2. Filtering datasets

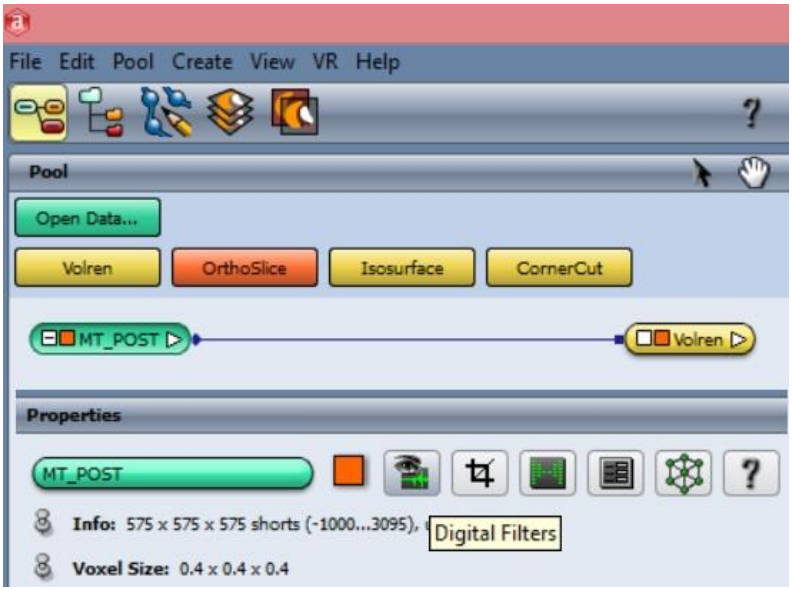

- Select the data item and from the “properties” menu in the down left hand side select “Digital filters”

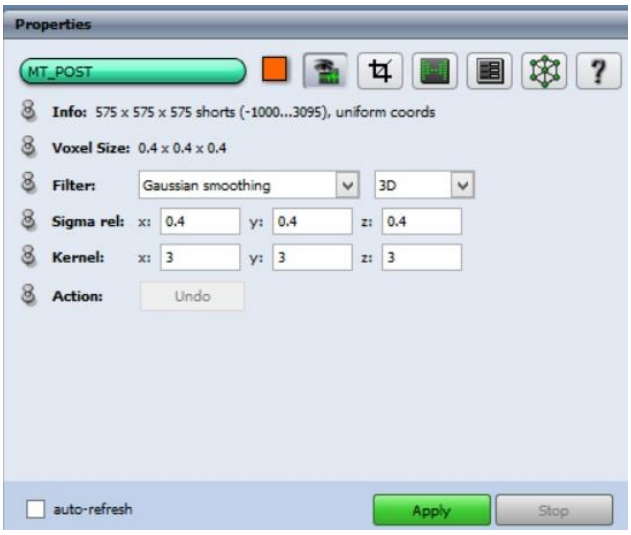

- Select “Gaussian smoothing and 3D “option and click “Apply”.

3. Cropping of datasets

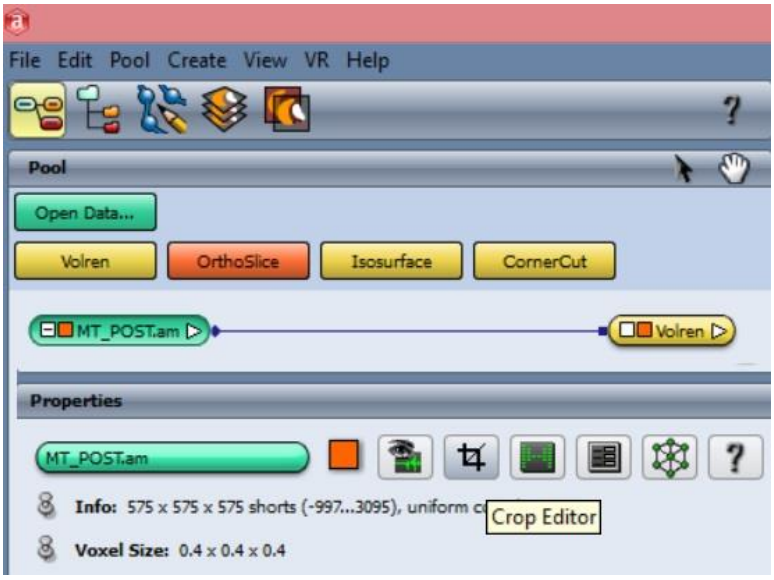

- After selecting the data item, navigate to “Crop Editor” in the properties section.

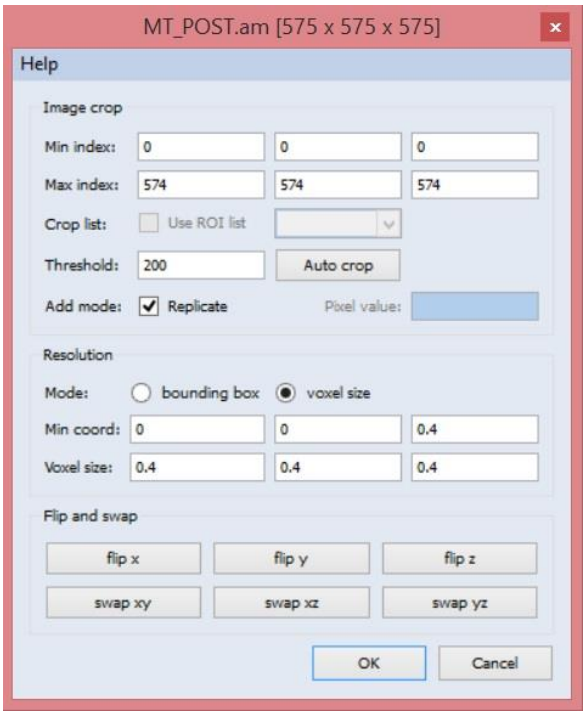

- Window as shown above appear and cropping box appears on the 3D volume.
- Resize the bounding window and click “OK” to commit.

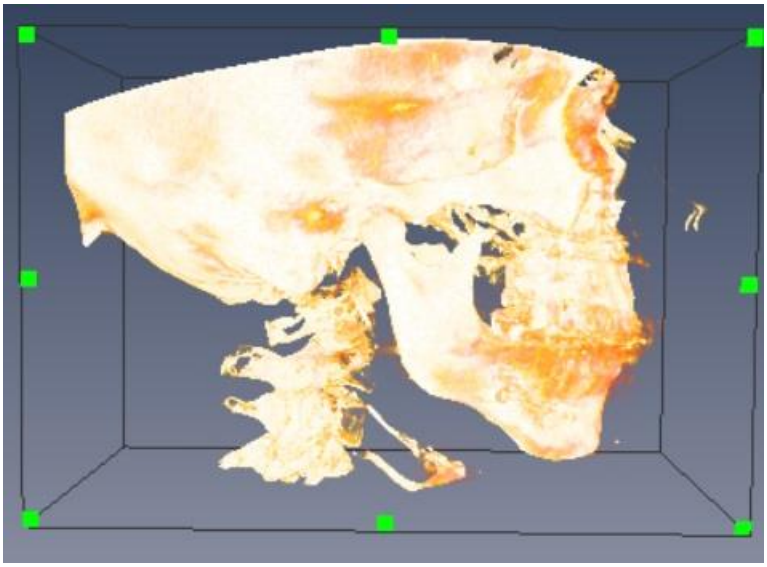

- Remember to save the data and network from time to time.

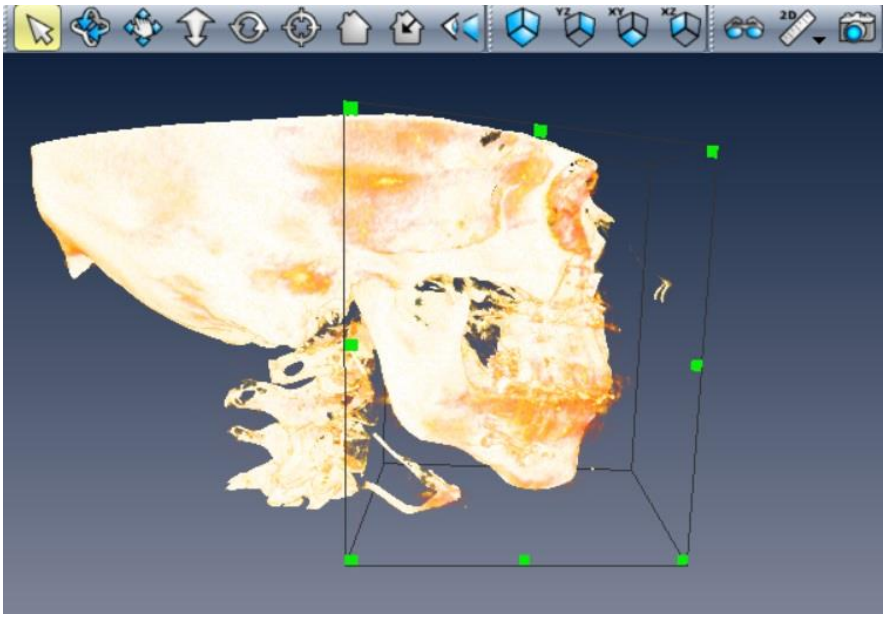

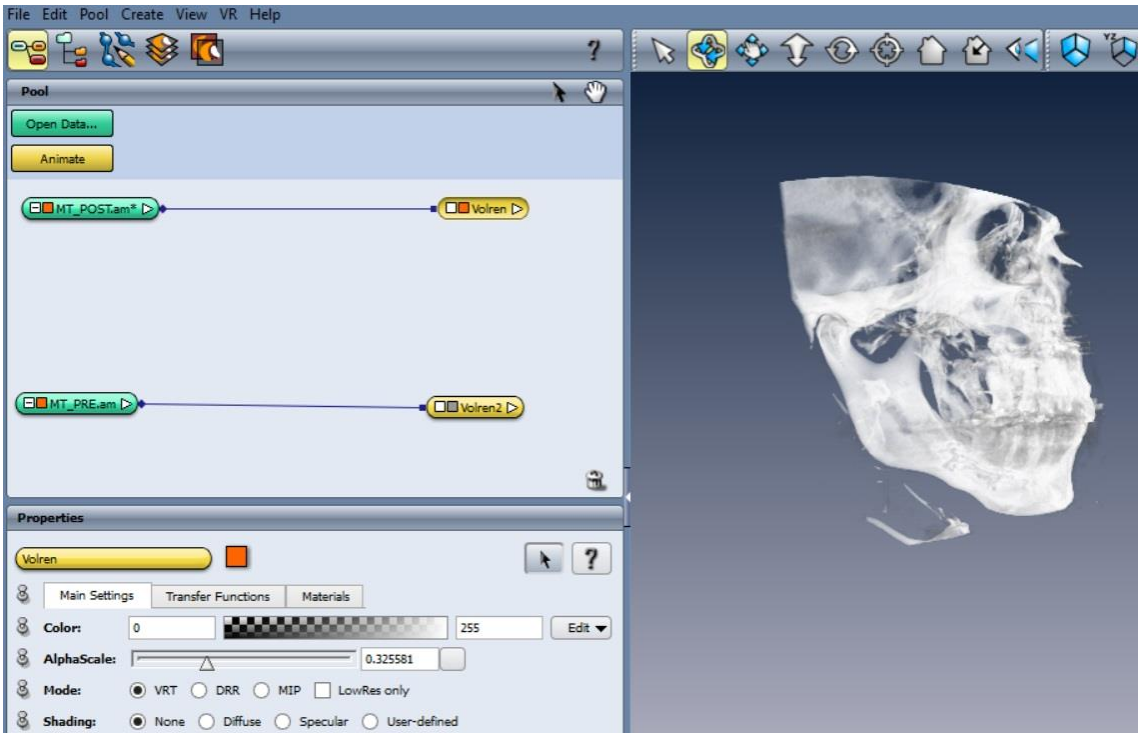

- After cropping under the properties section click on edit and select "grey.am" to change the volume into grayscale. As shown in the above figure.
- "Alpha scale" changes the transparencies.
- Repeat the process for both the process.

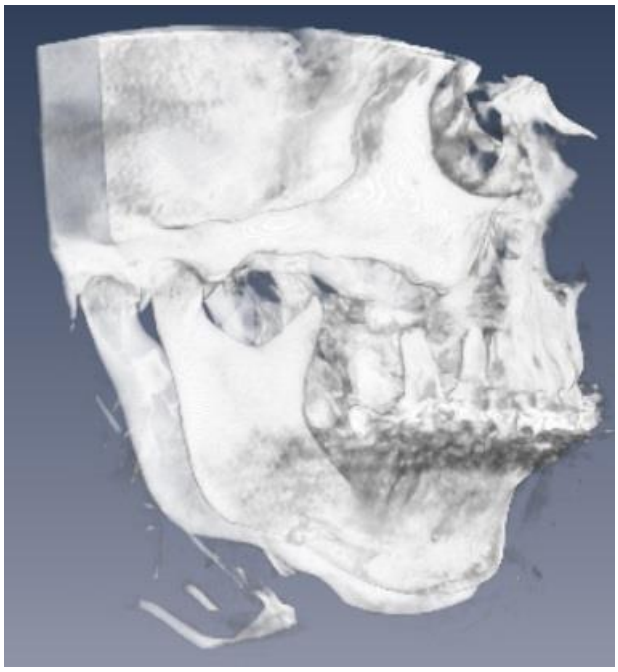

- At this point dataset must look as shown above.

4. Registration of images

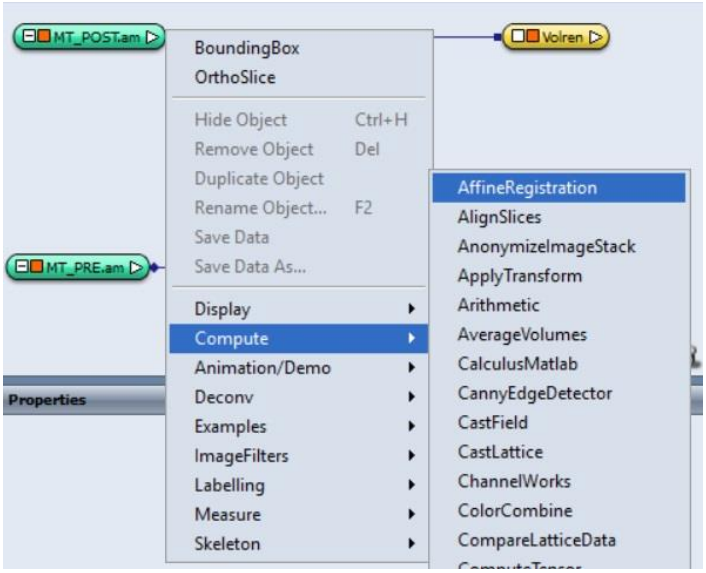

- Select the data item (MT_POST.am), and navigate to Affine registration as shown in the above figure.

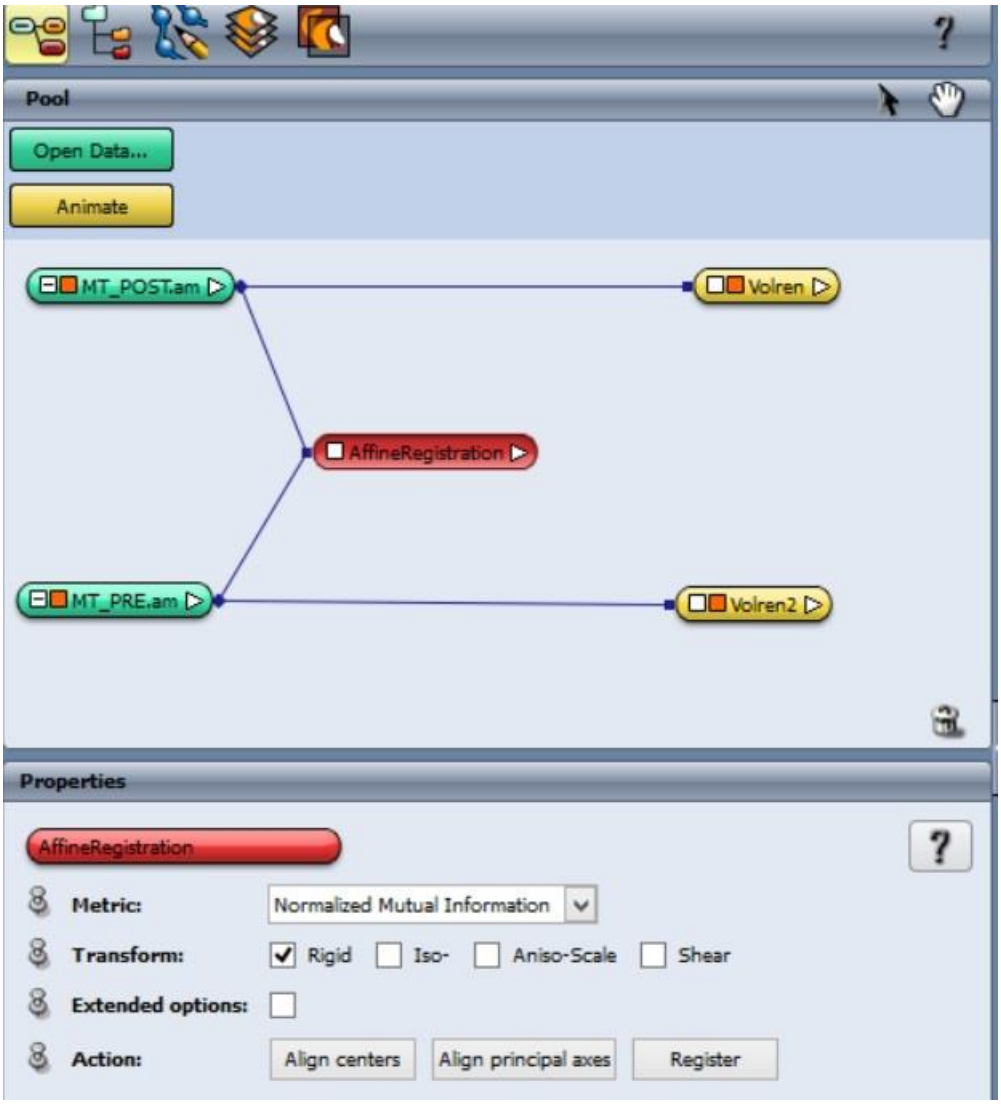

- Red object with “AffineRegistration” appears.
- Click on the square box in the red object and reference to other data item.
- The network should look like above.
- Then proceed to register the dataset by clicking on the “Register” button in the properties item.
- It should take about 2 minutes to complete the process.

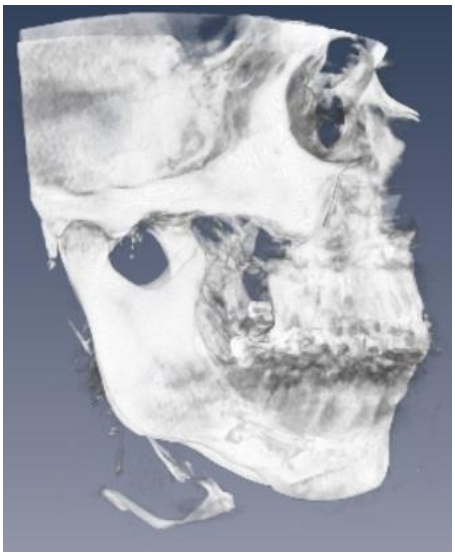

- Dataset after registration looks like above.

5. Segmentation

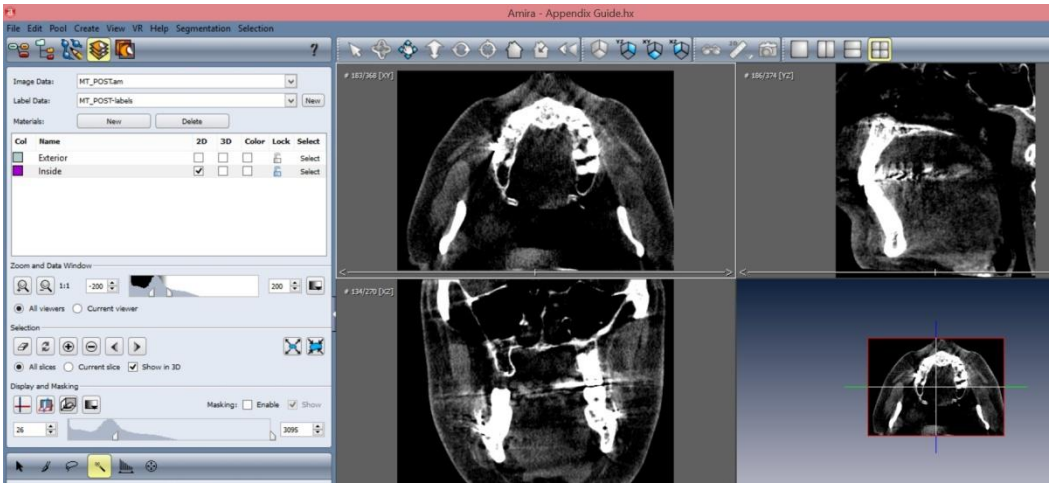

- Select the data item on navigate to Labelling->LabelField.
- The above interface will be shown.

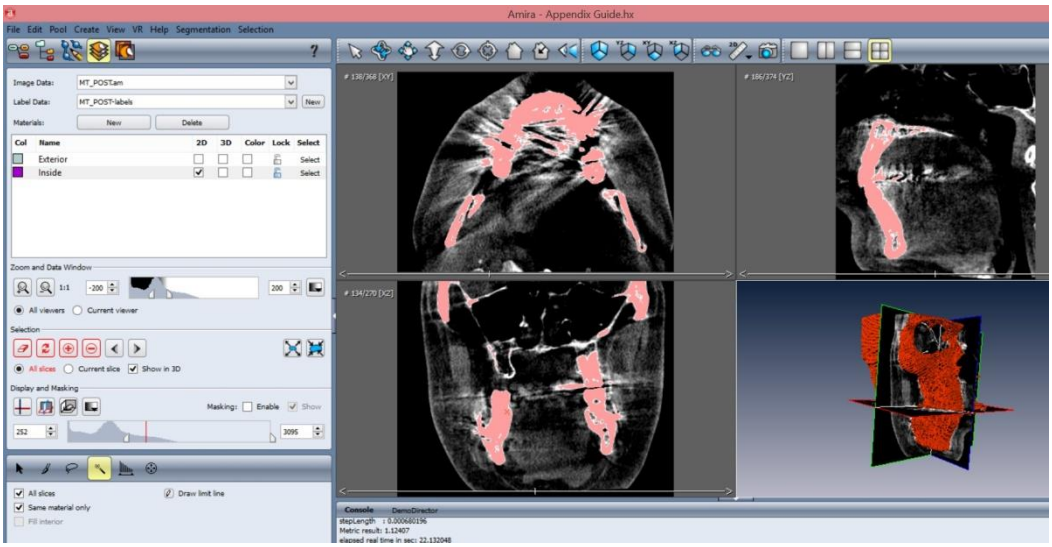

- Make the selection as per above screenshot.
- Magic wand, all slices and same material must be selected.

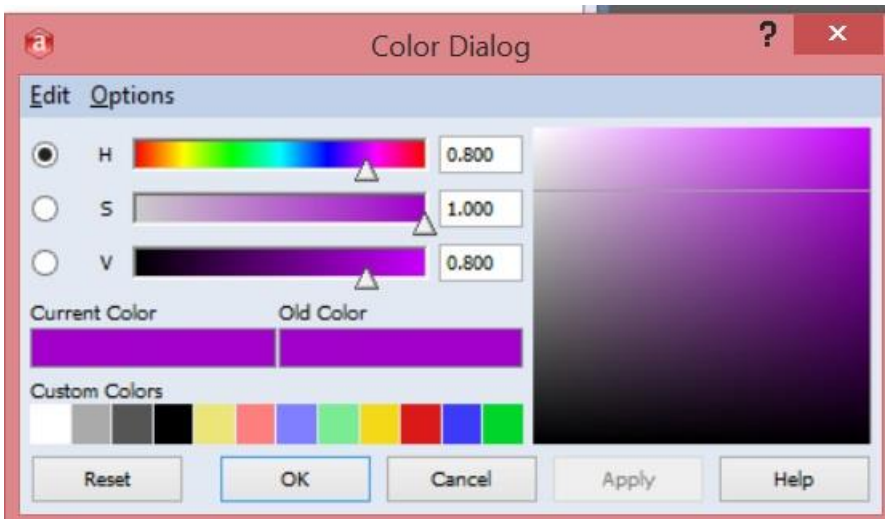

- Select a color for the model.

- Click on “+ “button to commit the segmentation.

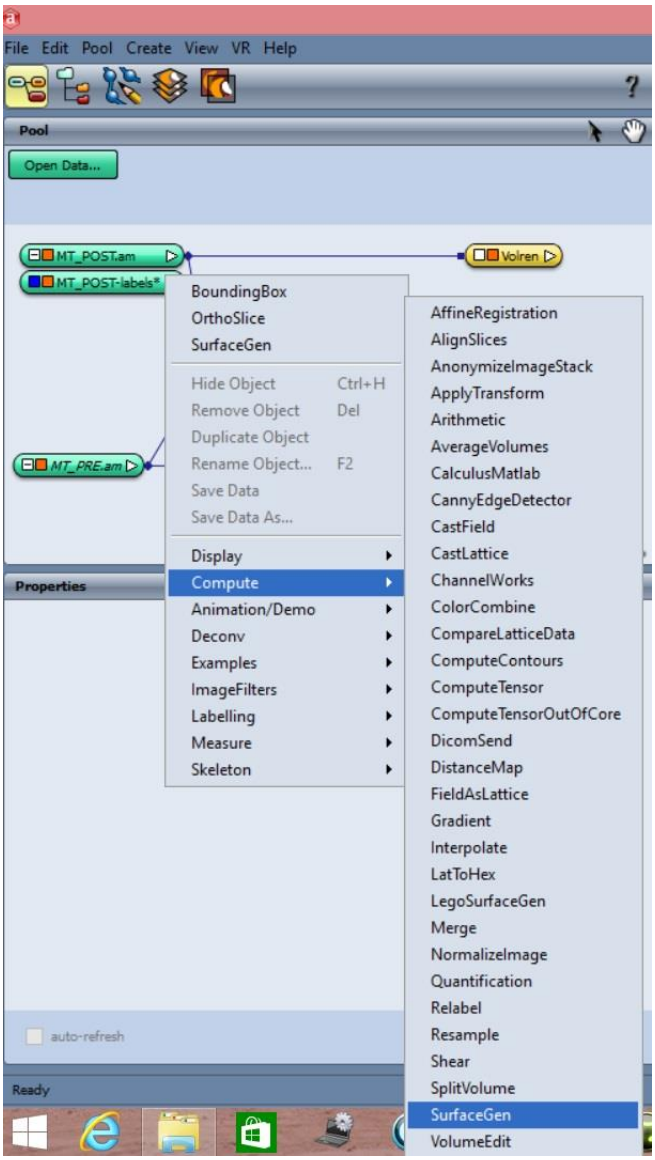

- Navigate to previous screen and select “SurfaceGen” as shown in the screenshot.
- A “.surf” object will be added to network pane.

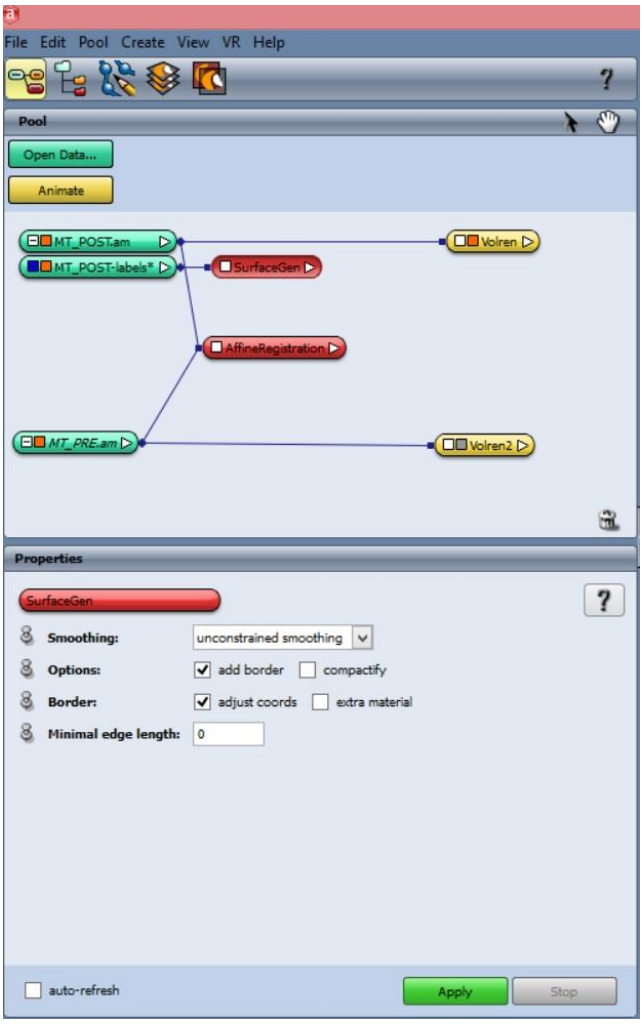

- Select “Apply” to create the 3D model.

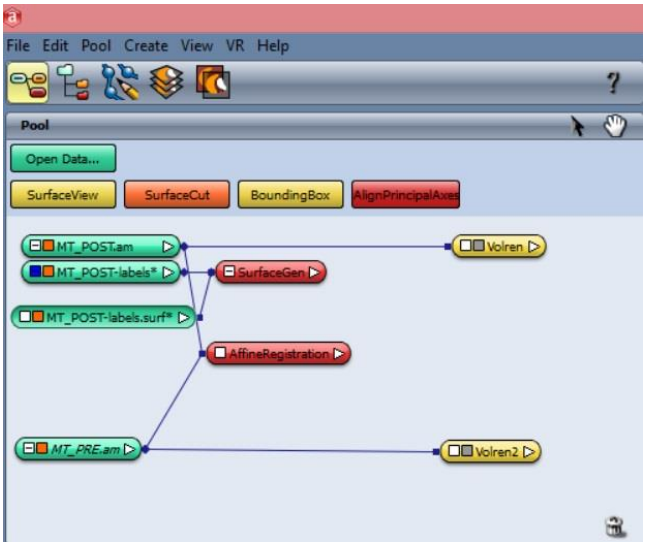

- Then select “SurfaceView” to generate the image volume.

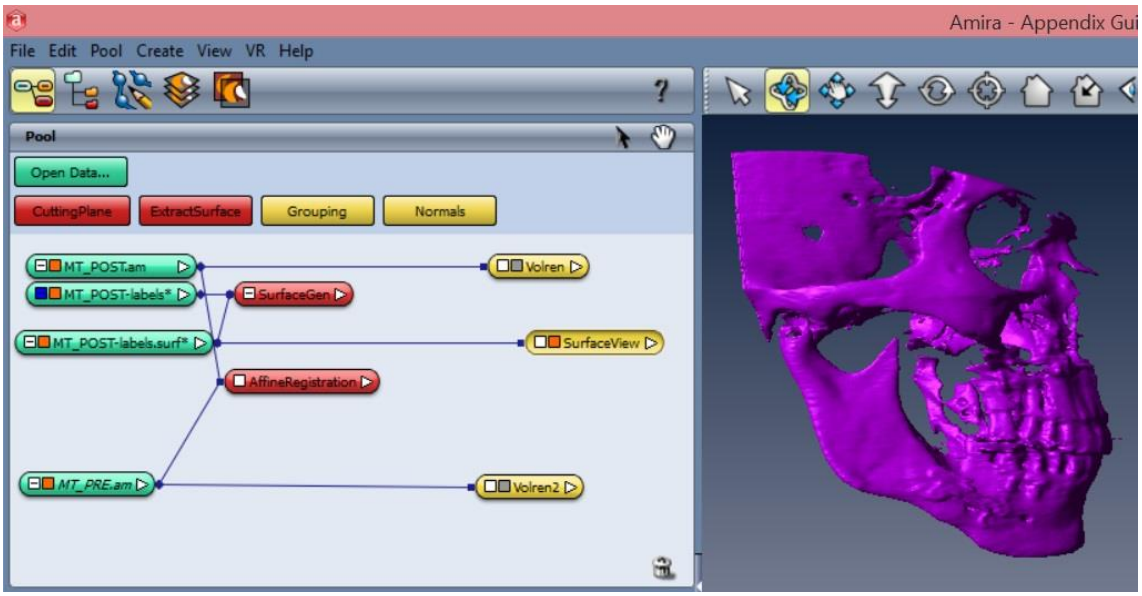

- The view and network so far should look like above screenshot.
- Click on "? "Button for detailed instructions.

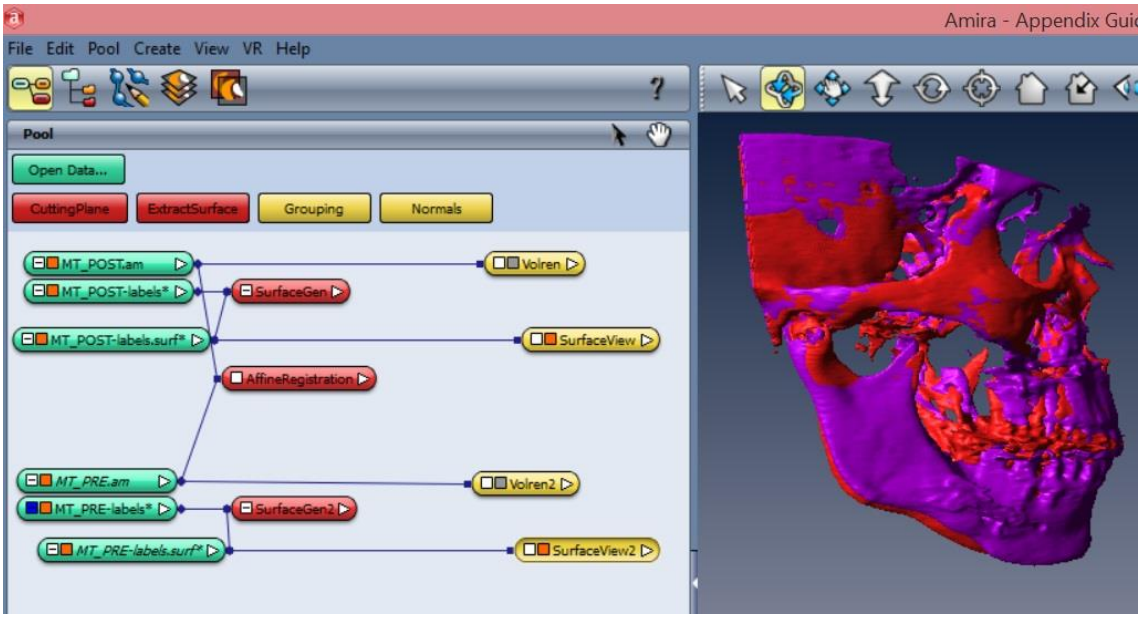

- Repeat the process for both the data scans.
- The 3D models should automatically look like above and overlapped.

6. Landmarks placement

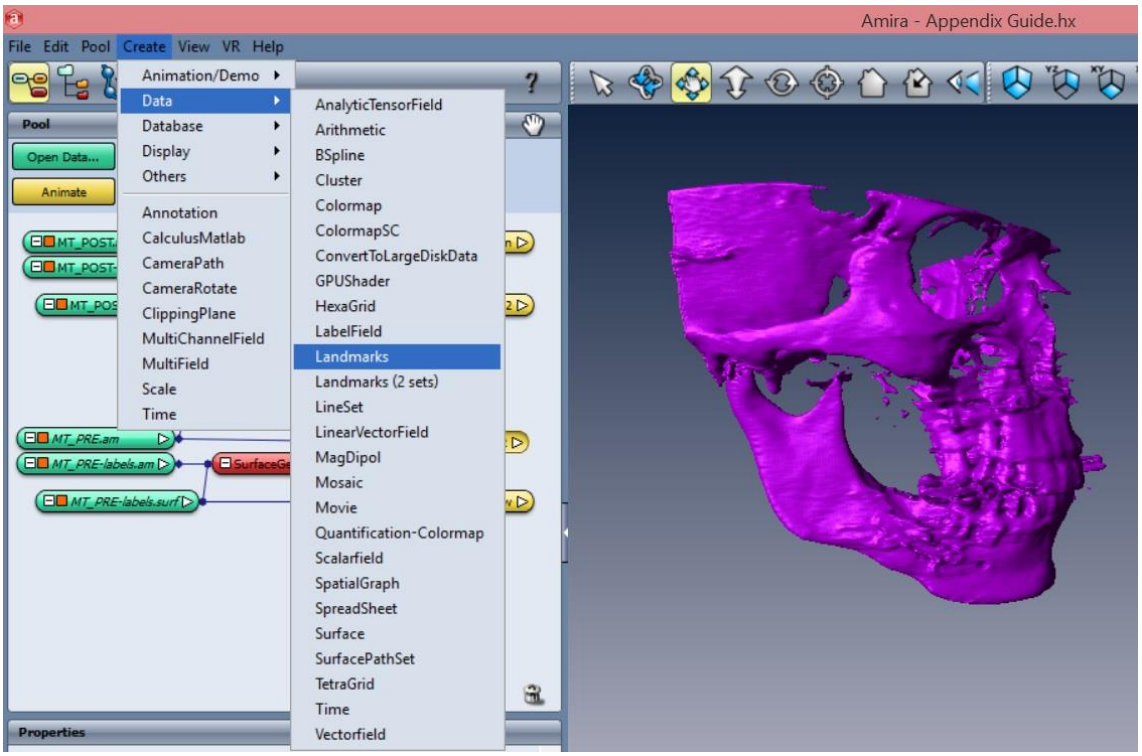

- Under “Create” navigate to Data->Landmarks.

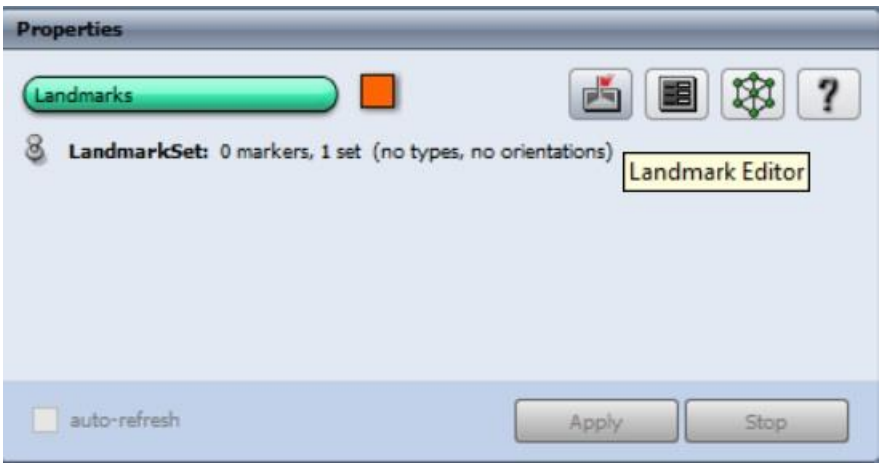

- Select “Landmark Editor” to start placing the landmarks on the 3D model.

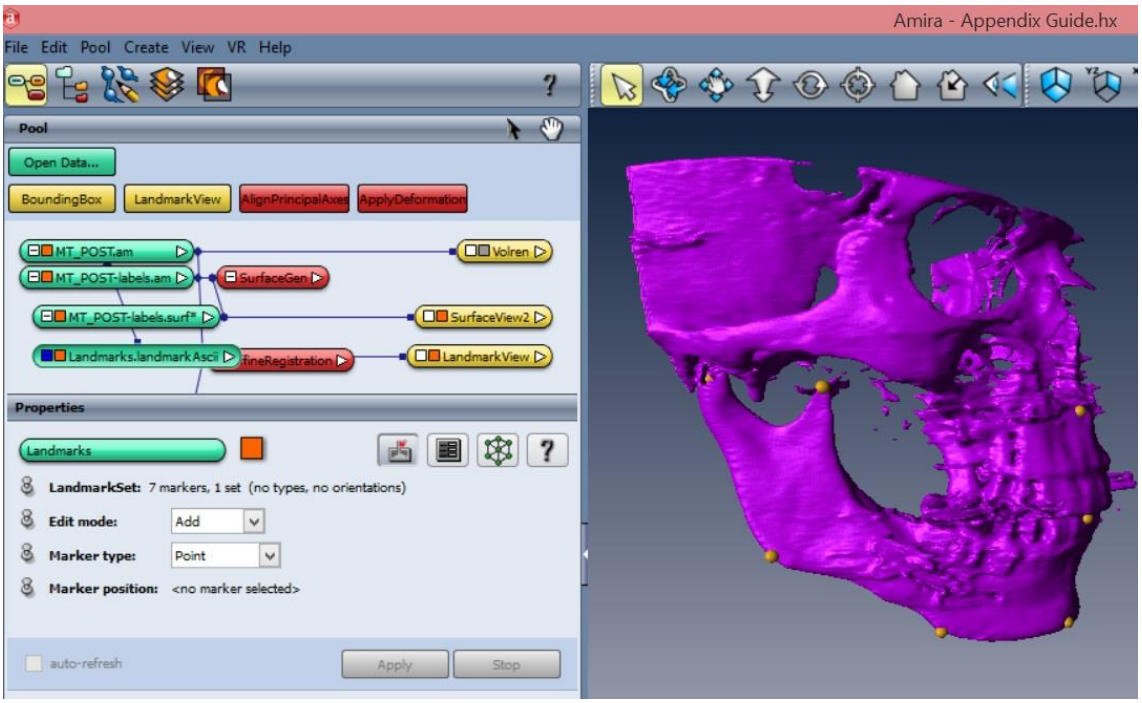

- Use the rotation and translate tools in the interface to change the 3D orientation and place the landmarks on the region of interest.

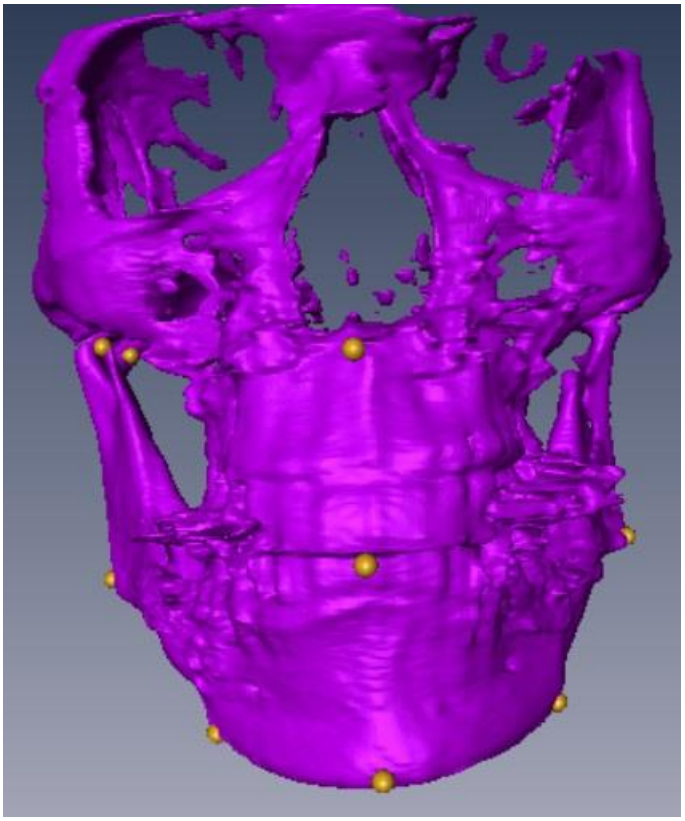

- After placing the landmarks 3D model should be similar to above shown model.

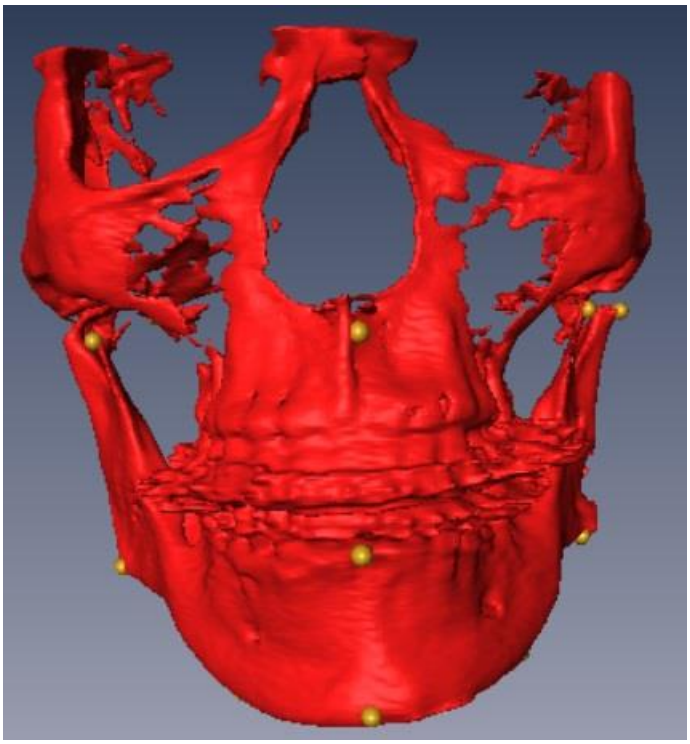

- Repeat the landmarks placement for both the data scans.

7. Inter-landmarks mapping

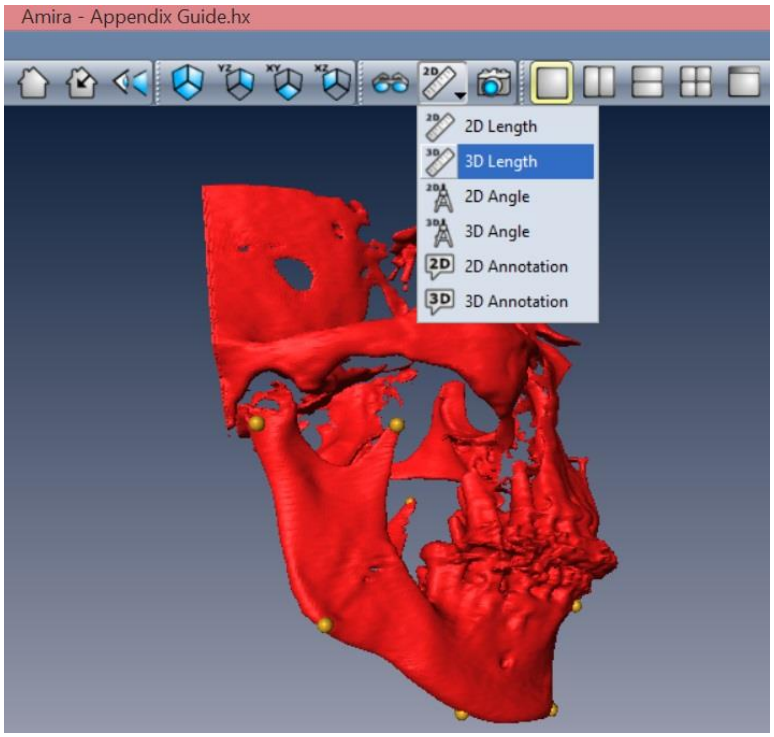

- Navigate to “3D Length” and start the mapping process between the landmarks.

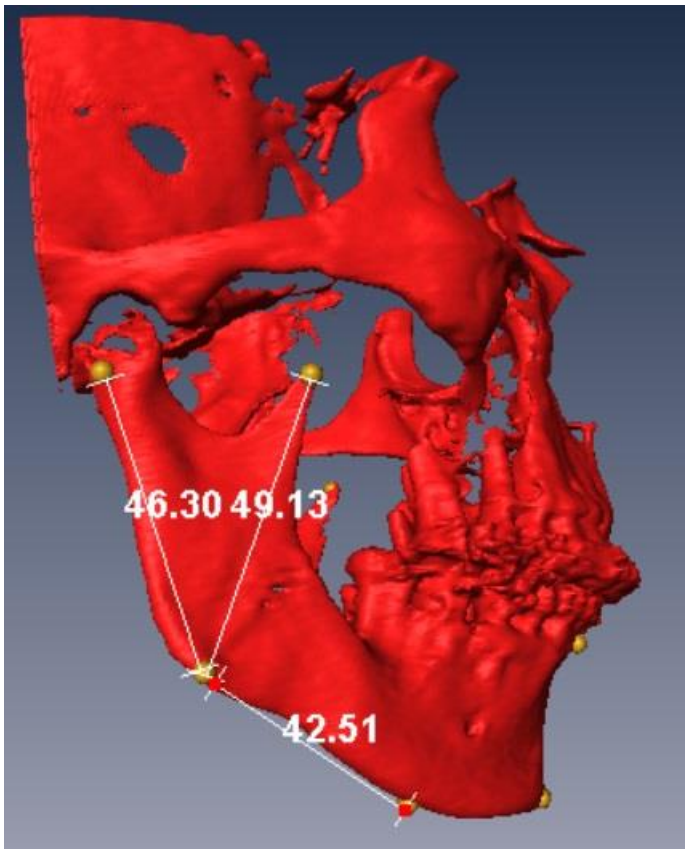

- The units are shown in millimeters or as per the specification of the image resolution.

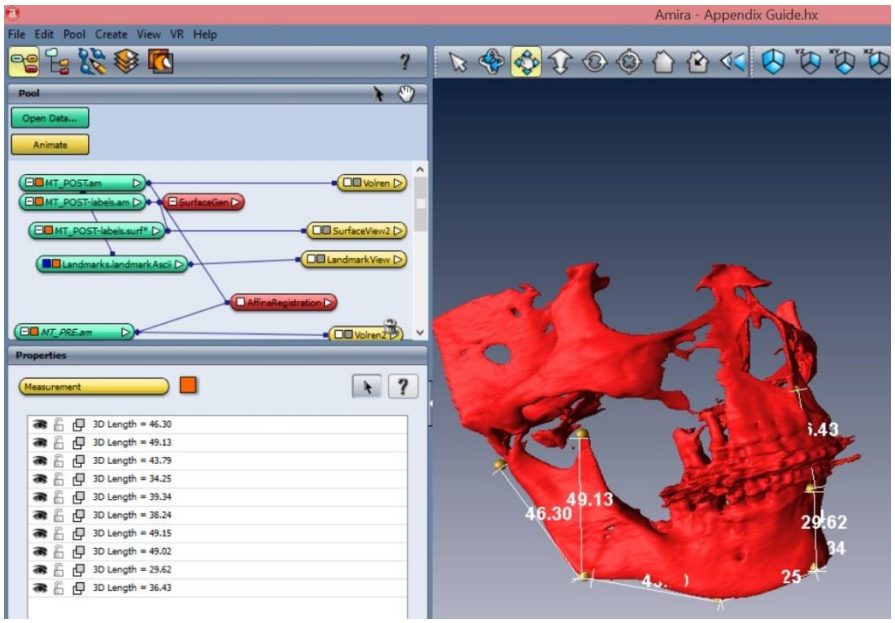

- Inter-landmarks distances are shown as a list

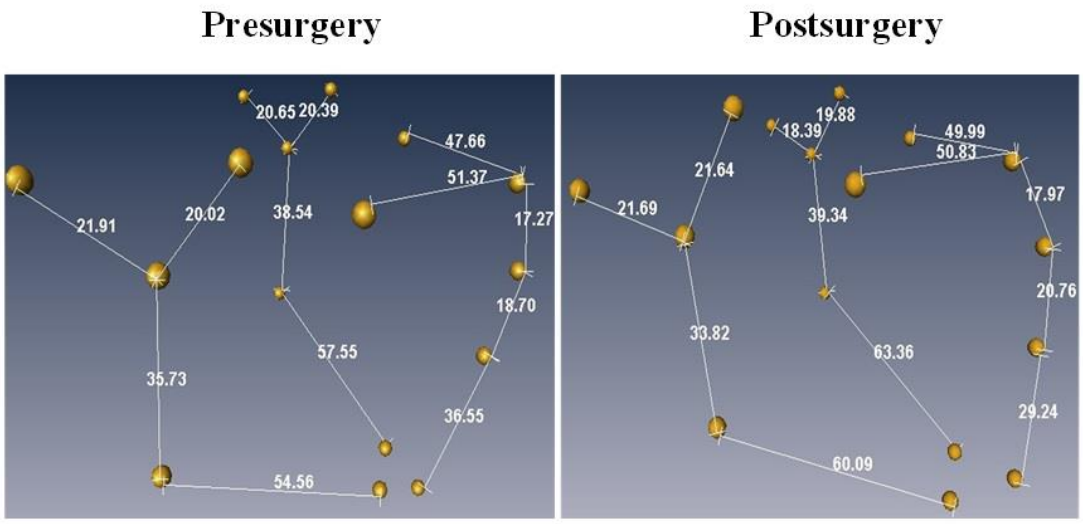

- The selection structure after mapping for both the models is shown above.

Note: The application has a guide button with detailed instructions for each module. These can be accessed by clicking on  anytime.